Indonesian Throughflow as a preconditioning mechanism for submarine landslides in the Makassar Strait

Rachel E. Brackenridge[1,2], Uisdean Nicholson[1]*, Benyamin Sapiie[3], Dorrik Stow[1] and Dave R. Tappin[4,5]

[1]School of Energy, Geoscience, Infrastructure and Society, Heriot-Watt University, Edinburgh EH14 4AS, UK

[2]School of Geosciences, University of Aberdeen, Aberdeen AB24 3FX, UK

[3]Faculty of Earth Sciences and Technology, Institut Teknologi Bandung, Indonesia

[4]British Geological Survey, Keyworth, Nottingham NG12 5GG, UK

[5]Department of Earth Sciences, University College London (UCL), London, UK

REB, 0000-0002-0572-314X; UN, 0000-0003-0746-8549; DRT, 0000-0003-3186-8403

*Correspondence: U.Nicholson@hw.ac.uk

Abstract: The Makassar Strait is an important oceanic gateway, through which the main branch of the Indonesian Throughflow (ITF) transports water from the Pacific to the Indian Ocean. This study identifies a number of moderate (>10 km^3) to giant (up to 650 km^3) mass transport deposits within the Makassar North Basin Pleistocene–Recent section. The majority of submarine landslides that formed these deposits originated from the Mahakam pro-delta, with the largest skewed to the south. We see clear evidence for ocean-current erosion, lateral transport and contourite deposition across the upper slope. This suggests that the ITF is acting as an along-slope conveyor belt, transporting sediment to the south of the delta, where rapid sedimentation rates and slope oversteepening results in recurring submarine landslides. A frequency for the >100 km^3 failures is tentatively proposed at 0.5 Ma, with smaller events occurring at least every 160 ka. This area is therefore potentially prone to tsunamis generated from these submarine landslides. We identify a disparity between historical fault rupture-triggered tsunamis (located along the Palu-Koro fault zone) and the distribution of mass transport deposits in the subsurface. If these newly identified mass failures are tsunamigenic, they may represent a previously overlooked hazard in the region.

The Indonesian Archipelago is seismically active due to its location at the intersection of four major tectonic plates. Earthquakes, volcanic eruptions and tsunamis represent significant geological hazards across the island nation. Of these natural hazards, tsunamis pose a specific risk to the sustainability and resilience of coastal communities. There have been a number of devastating Indonesian tsunamis over the last 15 years, triggered by various mechanisms. The 2004 megathrust earthquake and tsunami offshore Sumatra resulted in over 220 000 fatalities across the Indian Ocean region, 165 000 of these on Sumatra, making it one of the worst natural disasters of the last 100 years (National Geophysical Data Center/World Data Service, NGDC/WDS). The mechanism of the Palu tsunami (September 2018) is still uncertain but is proposed as a result of a combination of earthquake-related seafloor rupture and subaerial/submarine landslides (Carvajal *et al.* 2019; Takagi *et al.* 2019). Two surges, with maximum wave heights of over 10 m (NGDC/WDS), were recorded. Over 4000 fatalities occurred as a result of tsunami surges and widespread onshore liquefaction due to seismic shaking (Sangadji 2019). The Palu event was closely followed in December 2018, by the Anak Krakatau tsunami, where flank collapse, probably triggered by the erupting volcano, resulted in tsunami run-up of 30 m and over 400 fatalities on the local coasts of Java and Sumatra (NGDC/WDS; Grilli *et al.* 2019). The high number of fatalities of these two events has been attributed to the limited understanding of tsunami generation from mechanisms other than fault rupture and the lack of an effective tsunami warning system for non-seismic events (Yalciner *et al.* 2018; Williams *et al.* 2019).

The Makassar Strait has the highest frequency of tsunamis in Indonesia (Prasetya *et al.* 2001). Historical records show that most are caused by earthquake-generated fault rupture of the seafloor, with the exception of the September 2018 Palu event, which probably had a landslide component (Jamelot *et al.* 2019). However, there are numerous other factors in the Strait that could make it susceptible to submarine landslide-triggered tsunamis,

From: Georgiopoulou, A., Amy, L. A., Benetti, S., Chaytor, J. D., Clare, M. A., Gamboa, D., Haughton, P. D. W., Moernaut, J. and Mountjoy, J. J. (eds) 2020. *Subaqueous Mass Movements and their Consequences: Advances in Process Understanding, Monitoring and Hazard Assessments*. Geological Society, London, Special Publications, **500**, 195–217. First published online April 1, 2020, https://doi.org/10.1144/SP500-2019-171

including oversteepening of the continental slope due to carbonate growth and faulting, or sediment influx from the Mahakam Delta. The Strait is also the main channel for the Indonesian Throughflow (ITF), a strong current that transports 10–15 million Sverdrups (where 1 Sverdrup (Sv) = 1×10^6 m^3 s^{-1}) of water from the Pacific into the Indian Ocean (Kuhnt *et al.* 2004). Elsewhere, it has been shown that ocean currents and their associated deposits can precondition the slope for failure through rapid sediment deposition and erosion (Laberg and Camerlenghi 2008; Nicholson *et al.* 2020).

This study evaluates slope stability in the Makassar Strait, specifically the role of the ITF in preconditioning the slope for failure. Understanding the distribution of mass transport deposits (MTDs) that result from submarine landslides will allow us to identify specific regions of hazard and risk should these landslides be tsunamigenic. This has important implications for hazard mitigation and early warning systems across coastal regions of the Makassar Strait.

Geographical and oceanographic setting

Regional tectonic setting

The Makassar Strait separates the Indonesian islands of Kalimantan (Borneo) and Sulawesi in SE Asia (Fig. 1). It sits within a highly complex and dynamic plate tectonic setting (Daly *et al.* 1991), located at

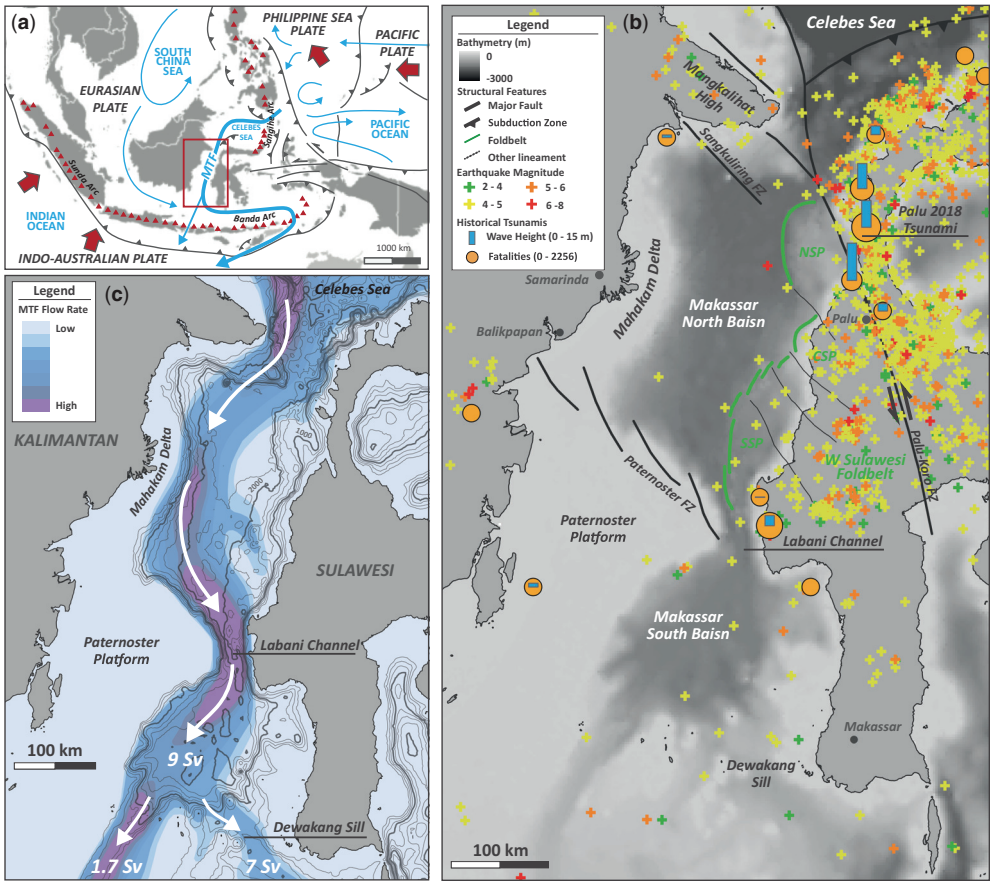

Fig. 1. (**a**) Regional tectonic and oceanographic setting. Study area indicated in red. MTF, Makassar Throughflow. (**b**) Structural features of the Makassar Strait from Puspita *et al.* (2005) (NSP, CSP, SSP refer to the Northern, Central and Southern structural provenances) and Cloke *et al.* (1999). SRTM30_PLUS Global Bathymetry Data from Becker *et al.* (2009). Historical earthquakes from the United States Geological Survey Earthquake Catalog (https://earthquake.usgs.gov/earthquakes). Historical tsunami data from the National Geophysical Data Center/World Data Service (NGDC/WDS) Global Historical Tsunami Database (NGDC/WDS). (**c**) Simulated daily average of Sv (Sv = 1×10^6 m^3 s^{-1}) for the main Makassar Throughflow jet between 52 and 420 m (Mayer and Damm 2012). Sv values from Kuhnt *et al.* (2004).

the intersection between four major lithospheric plates (Fig. 1a). The Indo-Australian Plate, located to the south of the Makassar Strait, is colliding with the Eurasian Plate in a northwards direction and is subducting below Sumatra and Java at a rate of *c.* 7 cm a^{-1} (Bergman *et al.* 1996; Koop *et al.* 2006). To the east, the large Pacific Plate interacts with the NW-moving (and clockwise-rotating) Philippine Sea Plate (Hall *et al.* 1995). As a result of plate interactions, a complex system of subduction, back-arc-thrusting, extension and major transform zones has developed (Hall 1997; Prasetya *et al.* 2001) (Fig. 1a). The region is extremely susceptible to seismic activity and volcanic arcs line the compressional plate boundaries, including the Sunda Arc and Banda Arc to the south and the Sangihe Arc to the NE (Katili 1975).

Due to its active plate tectonic setting, earthquakes are common across the Indonesian archipelago, with some associated with tsunamis. Along the Sunda Arc, historical tsunamis are generally generated by megathrust earthquakes. The mechanisms for these events are well understood and have been studied extensively following the devastating 2004 Indian Ocean tsunami (e.g. McCloskey *et al.* 2008; Okal and Synolakis 2008). Prasetya *et al.* (2001) show that the high frequency of historical tsunamis within the Makassar Strait, which is located away from any major subduction zone, is the result of shallow-depth earthquakes along the Palu-Koro transform fault zone (Fig. 1b).

Geological framework

The Makassar Strait forms a deep seaway that separates Kalimantan from Sulawesi. It varies in width from 100 to 200 km and is *c.* 600 km in length. It formed in the middle Eocene, when rifting and seafloor spreading was initiated (Hall *et al.* 2009). The onset of compression in the Late Miocene to Pliocene resulted in fold-and-thrust belt development along the margins of the Makassar Strait basins (Bergman *et al.* 1996). At present, far-field stresses and resulting faulting generate topographic features on the seabed, particularly in the east where Miocene–Pliocene compression has generated the West Sulawesi Fold Belt (Puspita *et al.* 2005). The Palu-Koro fault zone is a NNW–SSE-trending strike-slip fault and connects with the North Sulawesi Trench in the Celebes Sea. It crosses the Makassar Strait at its narrow northernmost opening, separating it from the Celebes Sea (Prasetya *et al.* 2001). The NW–SE-trending Eocene Paternoster fault zone acts as a topographic barrier separating the North and South Makassar basins (Fig. 1b).

The North Makassar Basin is north–south trending, 340 km long and 100 km wide, with water depths of 200–2000 m (Fig. 1b). The South Makassar Basin shows a similar range of water depths, is 300 km long, 100 km wide and NE–SW trending. The margins of the Makassar Strait show contrasting characteristics. To the west, the Paternoster Platform forms a wide shelf less than 200 m deep. This shelf has been periodically exposed during glacial conditions to form part of the Sundaland landmass, connecting Kalimantan, Java and Sumatra with the Asian continent (Bird *et al.* 2005; Hall 2009).

In the east of the Makassar Strait two fold belts are expressed as topographic features on the seabed (Fig. 1b). Puspita *et al.* (2005) define a Northern (NSP) and Southern (SSP) fold belt separated by a Central Structural Province (CSP). They note the different characteristics of the two fold belts, with the northern showing a steep western deformation front and a chaotic internal seismic character, whereas the southern shows well-developed thin-skinned fold-and-thrust deformation. These differences are attributed to interaction with basement structures and sediment supply, with the NSP likely consisting of muddier sediment (Puspita *et al.* 2005).

Studies of the active sedimentary systems within the Makassar Strait are limited but reveal a complex distribution of different depositional systems. Shallow-water sedimentation along the margins of the Makassar South Basin is largely carbonate dominated. The Paternoster Platform in the SW of the Strait forms a *c.* 40 000 km^2 medium- to coarse-grained carbonate sand sheet made up of bioclasts close to reefal build-ups, and benthic foraminifera in open marine regions (Burollet *et al.* 1986). The actively prograding Mahakam Delta is a major source of clastic sediment to the study area, with an estimated annual sediment discharge rate of 8×10^6 m^3 a^{-1} of clay, silt and sand-rich sediments (Roberts and Sydow 2003). Outboard and north of the delta front, carbonate deposition is found on the shelf edge, where a number of bioherm and shelf-edge build-ups are identified on bathymetry and seismic data (Roberts and Sydow 2003).

The continental slopes surrounding the Makassar Basins are locally fault-controlled (Guntoro 1999; Prasetya *et al.* 2001). Canyons are present on the steepest slopes, particularly in areas where sediment input into the basin is restricted. MTDs are identified at the foot of the slope and are generated by sediment failure (Saller and Dharmasamadhi 2012). Outboard of the Mahakam Delta, high sediment influx onto the slope has formed sinuous channel-levee complexes (Saller and Dharmasamadhi 2012).

The Makassar Basin floor is smooth, with no evidence of tectonic disturbance (Puspita *et al.* 2005). Seismic mapping at the base of the slope in front of the Mahakam Delta shows a large number of deep-water depositional features, including turbidite channels, levees and splays, as well as significant

MTDs (Posamentier and Meizarwin 2000). Sediment waves are a common feature, with Decker *et al.* (2004) attributing those along the Sulawesi Slope Apron to non-channelized hyperpycnal or turbidite flows triggered by storm events.

Oceanographic setting

The ITF is made up of numerous branches sourced from the Pacific Ocean. The main branch, the Makassar Throughflow (MTF), constitutes around 80% of water transfer (Fig. 1a) (Gordon *et al.* 2008) making the Makassar Strait the main location for water and heat exchange between the two oceans. The MTF exits the North Pacific between the Philippines and New Guinea and enters the Makassar Strait via the Celebes Sea (Tillinger 2011), where an average of 9.3 $\pm$ 2.5 Sv of water are transferred (Kuhnt *et al.* 2004) (Fig. 1c). It then splits into two branches, one of which flows through the Lombok Strait, between the islands of Bali and Lombok, and the other through the Timor Sea, between Timor and Australia (Fig. 1a, c) (Kuhnt *et al.* 2004). The Makassar Strait is the only low-latitude ocean gateway in the global ocean 'conveyor belt' of thermohaline circulation and is, therefore, a critical regulator of global oceanic energy exchange (Gordon and Fine 1996; Kuhnt *et al.* 2004; Rahmstorf 2007).

Within the Makassar Strait, moorings (Susanto and Gordon 2005) and modelling (Mayer and Damm 2012) show the MTF to act as a western boundary current along the Kalimantan continental slope. The flow of the surface 50 m is primarily wind-driven, with average velocities of 0.5 m s^{-1} (Gordon *et al.* 2008). Velocities increase with depth, reaching a maximum of around 1 m s^{-1} within a subsurface 'jet' extending down to 300 m, with a core corresponding to the thermocline, at about 100–150 m (Mayer and Damm 2012). Below 300 m, velocities reduce to under 30 cm s^{-1} (Tillinger 2011). The depth and speed of this high-velocity water mass varies seasonally in response to monsoonal forcing. It shallows and intensifies during the SE and NW monsoon seasons (March–April and August–September) (Gordon *et al.* 2008). Locally in the Makassar Strait, the MTF exerts a control on sedimentation. Seismic mapping of the Mahakam Delta by Roberts and Sydow (2003) shows the fine-grained prodelta (at *c.* 40 m water depth) is deflected to the south due to interaction with the MTF, which can reach velocities of 80 cm s^{-1} at the delta front.

Data and methodology

Bathymetric data

This study is based on three multibeam echosounder bathymetry surveys, acquired by Gardline Geosurvey on behalf of TGS, for their Indonesian Frontier Basins programme. The TGS_MakN, TGS_MakS and TGS_Pat surveys (Fig. 2) were acquired between December 2006 and February 2007 and cover around 60 000 km^2 in total. The multibeam echosounder data have been gridded at 25 $\times$ 25 m resolution, with features enhanced by a shaded relief map (0° azimuth, 45° angle). Backscatter data, at 5 m resolution, were also used to inform interpretation. These data cover the shelf edge, at around 200 m depth, to the basin floor, at over 3000 m water depth.

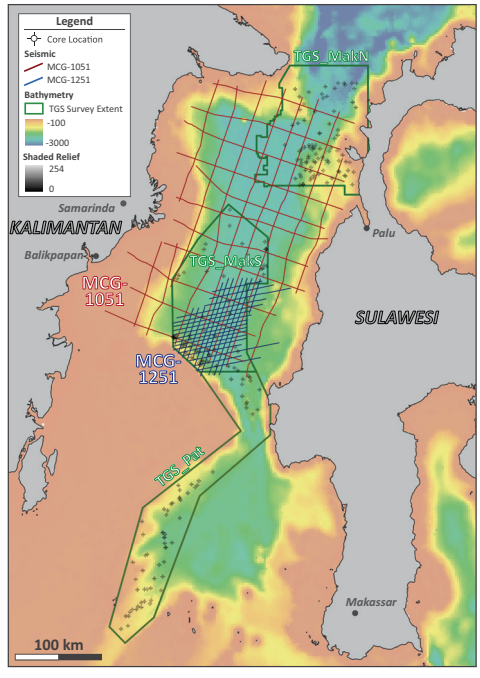

Fig. 2. Data used in the study. SRTM30_PLUS Global Bathymetry Data from Becker *et al.* (2009).

Additional bathymetric data, used for regional mapping (Fig. 2), include the Global Multi-Resolution Topography synthesis (Ryan *et al.* 2009) and the SRTM30_PLUS Global Bathymetry Data at 30 arc seconds resolution (Becker *et al.* 2009).

Slope gradient maps were extracted from bathymetric data and depth profiles generated to aid interpretation of physiographical domains. Structural lineations and depositional bodies were interpreted using bathymetric, slope and backscatter data to generate environment of deposition maps.

Seismic data

Two 2D seismic surveys from Multiclient Geophysical were interpreted in this study. The Makassar

Regional Super-Tie MCG2D Survey (MCG-1051) provides regional coverage of the Makassar North Basin (Fig. 2) with 21 2D pre-stack time migration (PSTM) seismic lines totalling *c.* 5000 km line length. The data were acquired in 2010 and processed by CGG Veritas in early 2011. The MCG-1051 survey was followed in 2012 by an infill survey (MCG-1251). The Makassar Infill 2D PSTM (Fig. 2) consists of 27 lines with a total of *c.* 2400 km line length. Both seismic surveys are high resolution in the upper few seconds below the seabed, which is the main section of interest in this study.

From the seismic data, we map Quaternary sediments deposited in the Makassar North Basin. Precise age constraints were not possible because of the lack of well control; however, a Top Pliocene horizon was interpreted based on del Negro *et al.* (2013). This allows us to date the age of the youngest sedimentary sequence at <2.6 Ma. Seismic data were interpreted using standard seismostratigraphic methods, and seismic facies (SF) were used to distinguish the different environments of deposition. Reflection terminations were used to identify key seismic stratigraphic surfaces, including tops and bases of individual MTDs. Due to the spacing of the 2D seismic data (17–40 km) only MTDs larger than *c.* 80 km^2 and 60 ms (*c.* 110–130 m thick) were mapped. Events smaller than 100 km^3 are under-represented due to limitations in spatial coverage of the 2D seismic survey, and the resolution for imaging thinner events. Seismic resolution deteriorates with depth; therefore, accurate mapping of MTDs was limited to the Pleistocene–Recent section. The volume of each MTD was calculated and converted to depth using a velocity of 2000 m s^{-1}, based on well velocity data gathered from MTDs of similar depositional character and burial depths in the Falkland Basin (Nicholson *et al.* 2020). An uncertainty range of 20% has been added to capture possible MTD velocities between 1800 and 2200 m s^{-1}. The total number of mapped landslides over the last *c.* 2.6 Ma was used to derive an average frequency for events of different volumes. As a result of the low seismic imaging resolution and line spacing, estimates of the frequency of smaller events (<100 km^3) are considered to be conservative.

Additional data

As part of the TGS-NOPEC Indonesian Frontier Basins programme, a number of additional datasets were acquired to complement the multibeam echosounder data used in the study. These data include gravity and magnetics acquired during the bathymetry survey, as well as regional gravity data compiled by Sandwell *et al.* (2014). Also, 234 piston cores were acquired within the region of the bathymetry survey (Fig. 2) in 2017 by TDI-Brooks International for geochemical analysis. From the cores over 600 samples were analysed for hydrocarbon indications. Shear strength measurements and basic sedimentary information were also available for each sample.

Historical earthquake data were compiled from the United States Geological Survey Earthquake Catalog (USGS; https://earthquake.usgs.gov/earthquakes, accessed May 2019). These records extend back to 1900 and list earthquake date, time, magnitude and epicentre depth. Historical tsunami data were downloaded from the National Geophysical Data Center/World Data Service Global Historical Tsunami Database (NGDC/WDS), which documents source location, date, time, event magnitude, maximum water height, total number of deaths, injuries and damage for each event.

Additional information was compiled from the literature where data coverage was unavailable for this study. Specifically, modelled routing of the MTF was georeferenced and digitized from Mayer and Damm (2012). Additional information about the features on the seafloor were gathered from studies by Fowler *et al.* (2004), Saller and Dharmasamadhi (2012) and Frederik *et al.* (2019).

Results and interpretation

Surface bathymetry interpretation

Physiographic domains. The main physiographic domains of the Northern Makassar Basin were mapped regionally on the SRTM30_PLUS Global Bathymetry Data (Becker *et al.* 2009). The continental shelf-slope break is defined by a change in slope gradient from less than 0.2° across the shelf, to slope gradients of 3–23° (Fig. 3). The shelf break occurs at *c.* 200 m water depth and varies significantly with distance from the coastline. To the west of the basin, a broad shelf of around 30–50 km extends out in front of the Mahakam Delta. This is significantly wider than the eastern shelf, which reaches a maximum width of 10–15 km and where a narrow, and locally very steep (up to 24°) continental slope grades to the basin floor (Fig. 3). The northern and southern limits of the basin are defined by structural highs (the Mangkalihat High and the Paternoster Platform respectively) which are bisected by deep, narrow channels. The deep Southern Makassar Basin is significantly smaller than the Northern Basin at approximately 180 km wide and 200 km in length (Fig. 3). This is a result of the extensive Paternoster Platform extending out from the Sulawesi Margin. Two channels connect the Southern Makassar Basin over the Dewakang Sill, to the Flores Sea in the South.

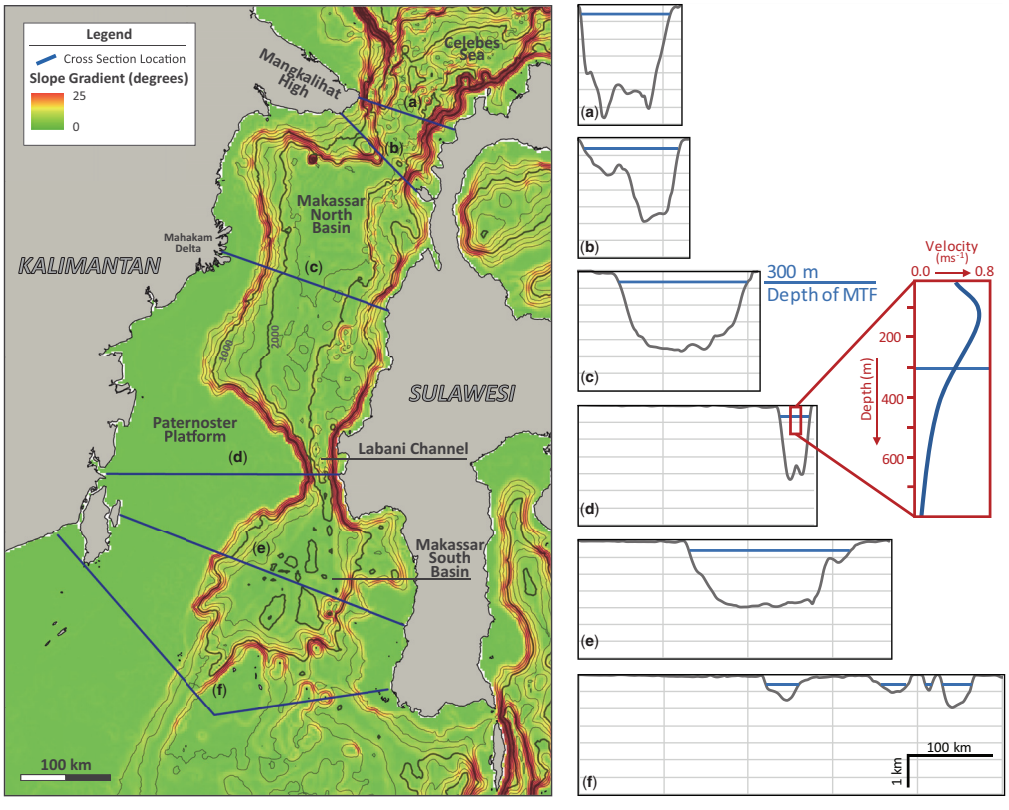

Fig. 3. Slope map extracted from the regional bathymetry RTM30_PLUS Global Bathymetry Data (Becker *et al.* 2009). Bathymetry contours at 250 m spacing). (**a–f**) Depth profiles across the Strait showing the main basin and channel features. Depth of Makassar Throughflow (MTF) indicated in blue. Velocity–depth profile shows average velocity profile for years 2004–09 (Susanto *et al.* 2012).

Structural features. The resolution of the SRTM30_PLUS Global Bathymetry Data (Becker *et al.* 2009) is insufficient to identify structural and sedimentary features in detail. However, the active tectonic nature of this region is evidenced by a number of features mapped on the high resolution TGS bathymetric surveys (Figs 4–6). Most notably, structural features include: (1) major strike-slip fault zones; and (2) fold-and-thrust complexes. The Palu-Koro fault zone is clearly imaged in the bathymetry data (Fig. 4). It extends from Palu Bay, Sulawesi, northwestwards to the northern edge of the Mangkalihat High. On the high-resolution TGS_MakN survey, the details of this fault zone can be mapped (Fig. 4). It is made up of multiple individual left-lateral strike-slip faults with both transtensional pull-apart and transpressional pop-up structures evident along the fault zone. The faults generate topography on the seabed of 250–300 m. The basin floor is modified in the east of the Makassar Strait where two fold-and-thrust belts are evident on the bathymetry, and a series of thrust-cored anticlines are clearly imaged on the seafloor (Fig. 4). Puspita *et al.* (2005) define two distinct fold-and-thrust belts named the Northern and Southern Structural Provinces (Fig. 1).

Sedimentary features. There is evidence for multiple downslope systems transporting sediment into the Makassar North Basin. From the backscatter data we interpret subtle sedimentary features, distinguishing bedrock or carbonates of high acoustic reflectivity (strongly negative values) from medium reflectivity sands and low reflectivity mud-dominated deposition (values close to zero) (Fig. 5). Dominant sedimentary features include: (1) slope canyons; (2) basin floor fans; (3) slope failure scarps; and (4) and deep-water turbidite channels.

The TGS_MakN bathymetric survey, on the eastern margin of the Makassar North Basin, images a deep-water channel in the northern fold belt (Fig. 4). The channel is sourced from the mouth of Palu Bay, which incises to a depth of 300 m in the upper slope, down to 600 m deep in its distal portion. The channel profile shows steep, erosive flanks,

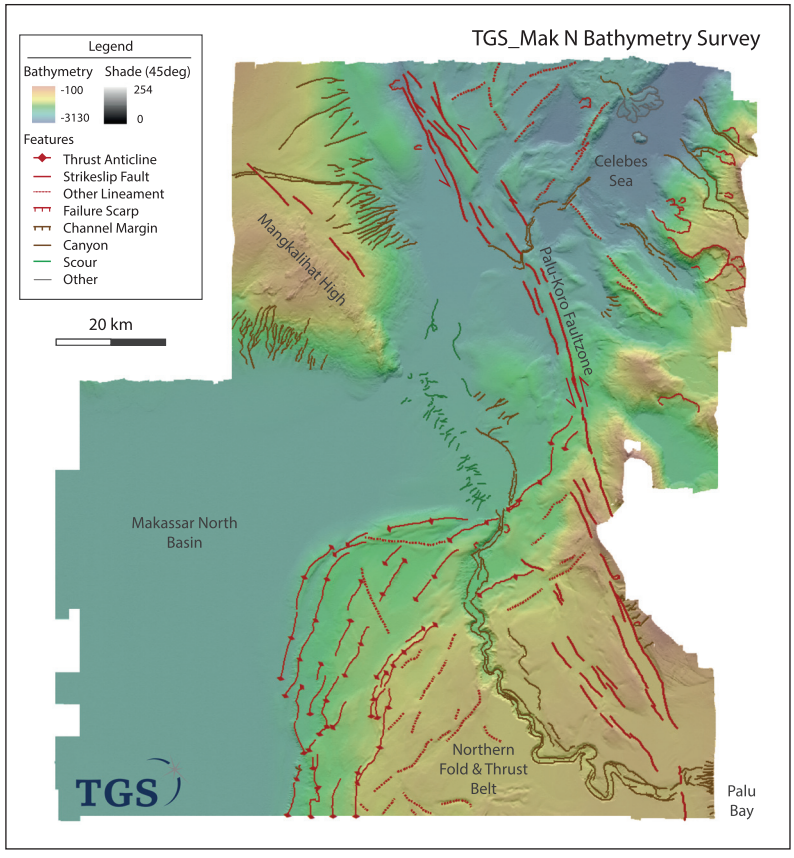

Fig. 4. Bathymetry data interpretation of the Makassar North TGS survey. Bathymetry data overlaying a shade map with interpretation of structural and sedimentary features. Survey location indicated on Figure 2.

bordering a flat channel axis. The channel shows a moderate sinuosity of 1.4, which is modified by thrust-cored anticlines in the outer part of the fold belt. There is no evidence for an associated depositional fan on the basin floor.

A downslope (turbidite) depositional fan is seen in the TGS_MakS bathymetric survey, where an extensive sediment wave field has developed along the eastern side of the basin. The Makassar South backscatter data image a small downslope channel *c.* 2.5 km wide, 200 m deep on the eastern continental slope, which feeds a sediment fan with low backscatter values compared to the surrounding basinal sediment (Fig. 5). The sediment wave field suggests periodic unconfined flow across the continental margin between the two fold-and-thrust belts. Wave crests are orientated parallel or slightly oblique to the continental slope. The sediment waves are sinuous with wave lengths of 0.5 to 1 km, and heights of 5–30 m. Backscatter data show higher values on the lee slide of waves.

Where sinuous channels and sediment waves dominate the eastern margin of the basin, v-shaped and straight canyons dominate on the northern, western and southern margins. High-resolution bathymetric data only cover a small portion of the continental slope of the Mangkalihat High and the Paternoster Platform. Both these continental margins show canyon systems of very different characteristics. The Mangkalihat High canyons are tightly spaced, straight, v-shaped downslope canyons that range between 40 and 80 m deep (Fig. 4). The TGS_MakS bathymetric data cover a number of canyons fed from the Paternoster Carbonate Platform. Here, four large v-shaped canyons (over 5 km wide, 400–700 m deep) are separated by slope-perpendicular 'spurs' (Fig. 5). This change in character may be due to clastic v. carbonate-dominated sedimentation and erosive processes in the north and south, respectively. We do not have access to high-resolution bathymetric data over the western continental slope of the Makassar North Basin;

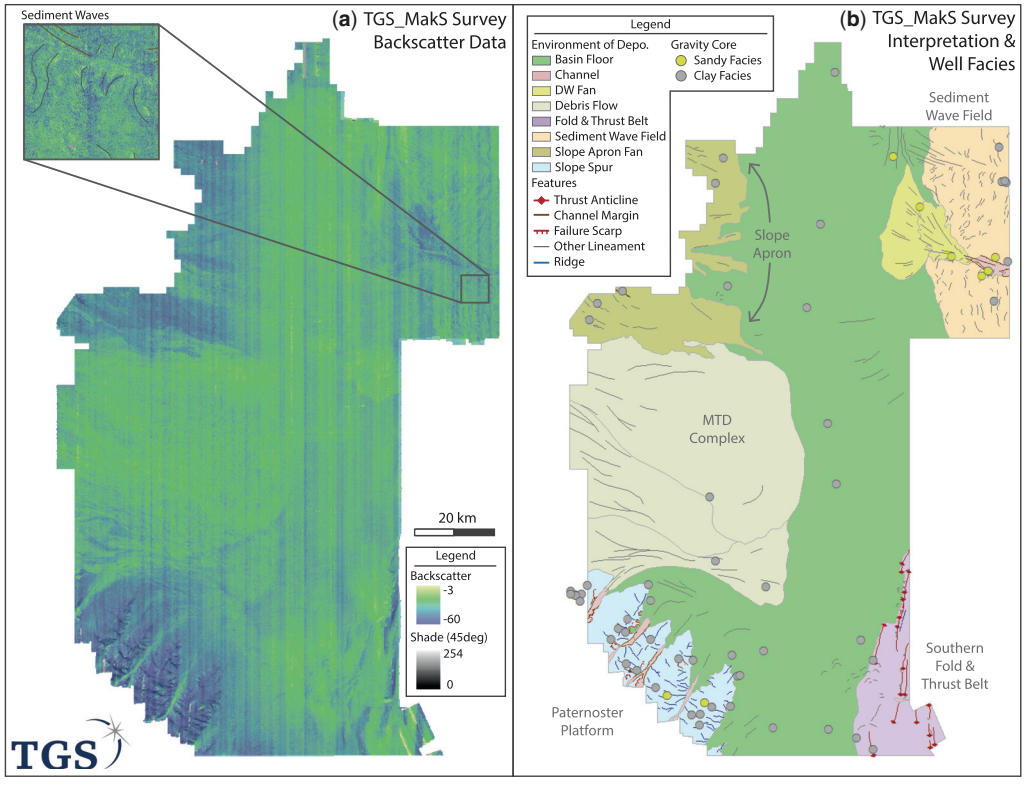

Fig. 5. Bathymetry data interpretation from the Makassar South TGS survey. (**a**) Backscatter overlaying a shade map. Highly negative values (indicated in blues) represent bed rock, carbonates or sands. Greens indicate mud-dominated deposition. Insert shows zoom-in of sediment wave crests. (**b**) Interpretation of sedimentary and structural features with seabed facies from piston cores. Survey location indicated on Figure 2.

however, published studies suggest that downslope canyons and associated slope apron fans are widespread (e.g. Fowler *et al.* 2004; Saller *et al.* 2008).

Small failure scarps (<5 km^2) are a common feature of the forelimbs of thrust belt anticlines (Fig. 6) and in the TGS_MakN bathymetric data to the north of the Palu-Koru Fault zone (Fig. 4). The backscatter imaging over the TGS_MakS bathymetric survey highlights a region of mass-transport deposition (Fig. 5). These deposits are characterized by low backscatter values, suggesting low acoustic reflectivity and therefore high mud content. Kinematic indicators, expressed as lineaments on the seafloor (Fig. 5b), suggest a flow direction from the west. Evidence for slope failure is also seen in the TGS_Pat bathymetric survey (Fig. 6). Large blocks (reaching 20–35 m in diameter) are distributed at the base of slope along the western margin of the Paternoster Platform in the Makassar South Basin (Fig. 6b).

The TGS_Pat bathymetric survey data image a number of features that we interpret as contourites. Immediately south of the Labani Channel, a scalloped, scour-like feature is imaged at 1300 m water depth (Fig. 6a). The feature is orientated perpendicular to the slope, with a steep lee and shallow stoss side; all characteristic of formation by alongslope erosion. To the south, there is an erosional terrace across the upper slope at 200 m water depth (Fig. 6b). This terrace is 700–800 m wide and is elongated alongslope for *c.* 10 km. It is formed along the north side of a large embayment. On the south side of this embayment, a mounded topographic feature around 500 m high is seen at the base of the slope. It is elongated alongslope, (Fig. 6a) and tentatively interpreted as a contourite mounded drift; however, further geophysical data are required to confirm this interpretation.

Subsurface seismic interpretation

Seismic tectonostratigraphy. The Top Pliocene was interpreted across the entire seismic survey and an isochron thickness map of the seabed to Pliocene

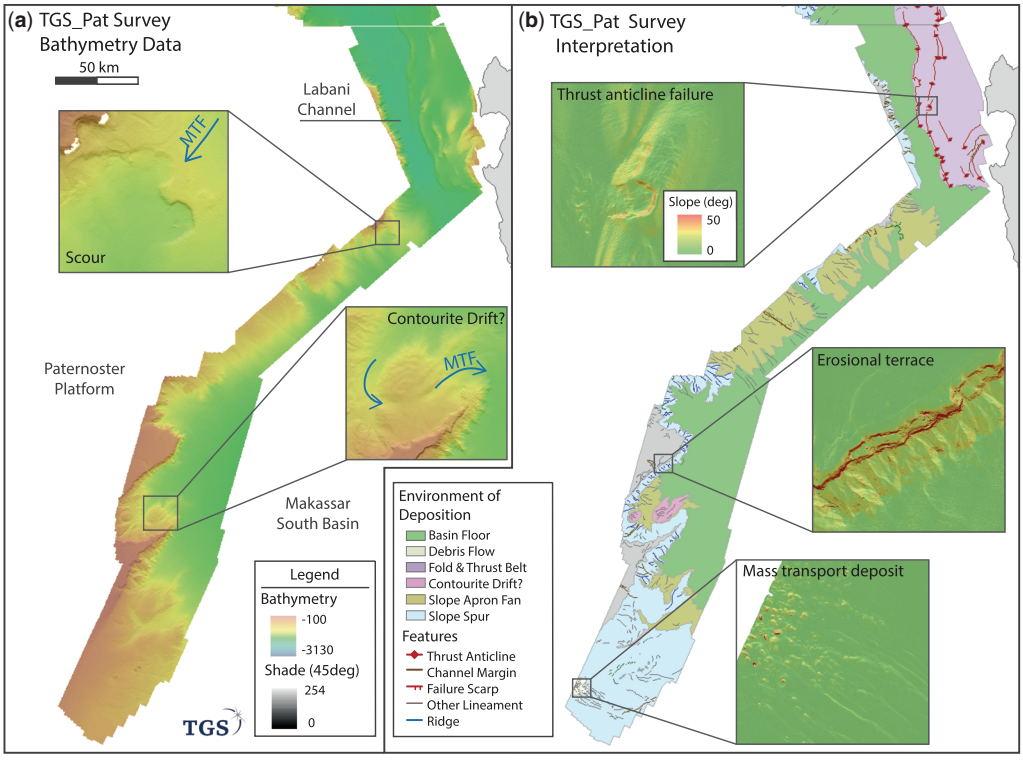

Fig. 6. Bathymetry data interpretation from the Paternoster TGS survey. (**a**) Bathymetry overlaying a shade map. MTF (inserts) indicates the direction of the Makassar Throughflow. (**b**) Interpretation of sedimentary and structural features. Inserts show slope gradient. Survey location indicated on Figure 2.

sequence generated to show depositional trends in Pleistocene–Recent sediments of the Makassar North Basin (Fig. 7). The isochron thickness map reveals a basin depocentre in the north, with a general thinning to the south. An additional depocentre is identified in the west on the edge of the data in front of the Mahakam Delta (Fig. 7).

Seismic facies and environment of deposition. SF interpretation identifies eight dominant facies (I–VIII) (Figs 8 & 9; Table 1). Each facies is characterized from its internal reflection character, continuity, amplitude and frequency, in addition to external morphology and/or bounding relationships (Table 1). The regional extent of each of the facies was mapped (Fig. 8). These observations were combined with those from the bathymetric mapping to interpret an environment of deposition for each facies (Table 1).

SF I. Two regions of polygonally faulted pelagic sediments (SF I) are located in the deepest part of the basin, directly in front of the two fold-and-thrust belts (Fig. 8). Here, high-amplitude, high-frequency reflections are offset due to densely spaced high-angle extensional faulting (Fig. 9 I). These faults are characteristic of sediment compaction and fluid expulsion from fine-grained biosiliceous sediments (e.g. Davies and Ireland 2011). These facies are associated with a prominent bottom-simulating reflector (BSR). Based on the polarity reversal of this BSR, and the polygonally faulted nature of the associated facies, we interpret this as a diagenetic Opal A/CT boundary zone within highly siliceous pelagic sediments (Lee *et al.* 2003). Polygonal faulting and a strong Opal A/CT transition suggest a high silica content, implying a lack of terrigenous sediments (turbidites, hemipelagic mud), allowing us to distinguish this facies from hemipelagites (see SF II).

SF II. High-amplitude, high-frequency, laterally continuous reflections with draping morphology are interpreted as hemipelagic facies (Fig. 9 II). SF II transitions towards the basin centre into SF I. Based on the lack of polygonal faulting and BSR, we interpret this facies as less biosiliceous, but still very fine-grained, hemipelagites.

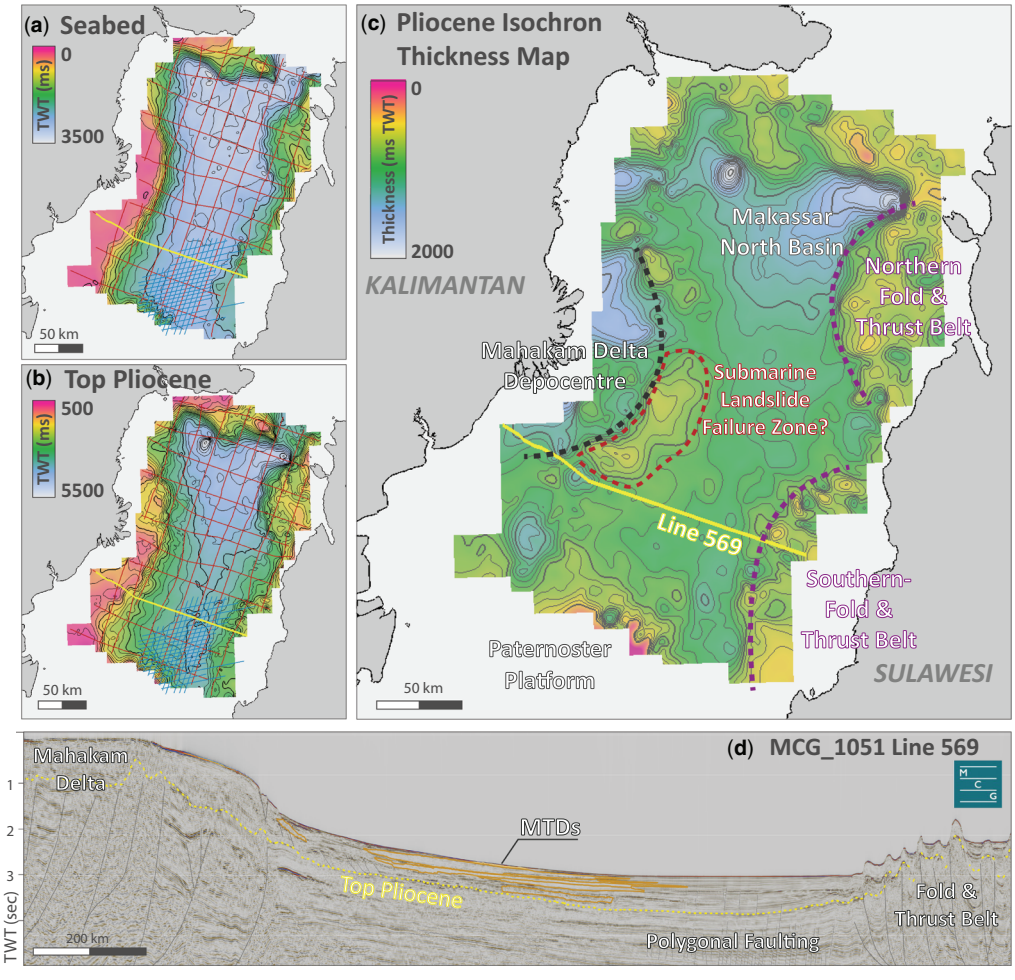

Fig. 7. (**a**)–(**c**) Seabed to Pliocene mapping and (**d**) example regional seismic line from the MCG-1051 survey.

SF III. Sediment waves are found locally on the western basin margin and an extensive sediment wave field dominates the eastern margin, between the two fold-and-thrust belts (Fig. 8). The waves are characterized by hummocky, subparallel, semi-continuous reflections (SF III) (Fig. 9 III). The package is 200–400 ms two-way travel time (TWT) in thickness and affects the seafloor bathymetry as seen in the Makassar North Basin (Fig. 5). The base of this seismic package is a high amplitude reflection showing opposite polarity to the seafloor. This is likely a BSR associated with gas hydrates that could have promoted gravitational movement (creep) downslope. The seabed topography generated by such a process appears to have promoted the growth of upslope-migrating sediment waves that have likely been deposited by unconfined downslope (turbiditic) processes.

SF IV. Dominating the Pleistocene basin fill are numerous MTDs, clearly identifiable from their semi-transparent and chaotic seismic signature (SF IV). The MTDs are characteristically deformed, chaotic, discontinuous and low amplitude (Fig. 9 IV). Rare internal reflections show extension in their proximal portions, and imbrication and compression in their distal parts (Fig. 10). Individual MTDs are mappable because they form lenticular bodies with erosional bases of negative acoustic impedance (AI), and a strong positive AI upper surface onto which younger stratigraphy onlaps (Fig. 10). MTDs thin and pinch out, upslope and laterally. Their downslope extent is either thinning (e.g. Fig. 10), or shows an abrupt, stepped change in facies. SF IV is predominantly distributed along the western side of the basin, with the largest events clustered in the SW (Fig. 8).

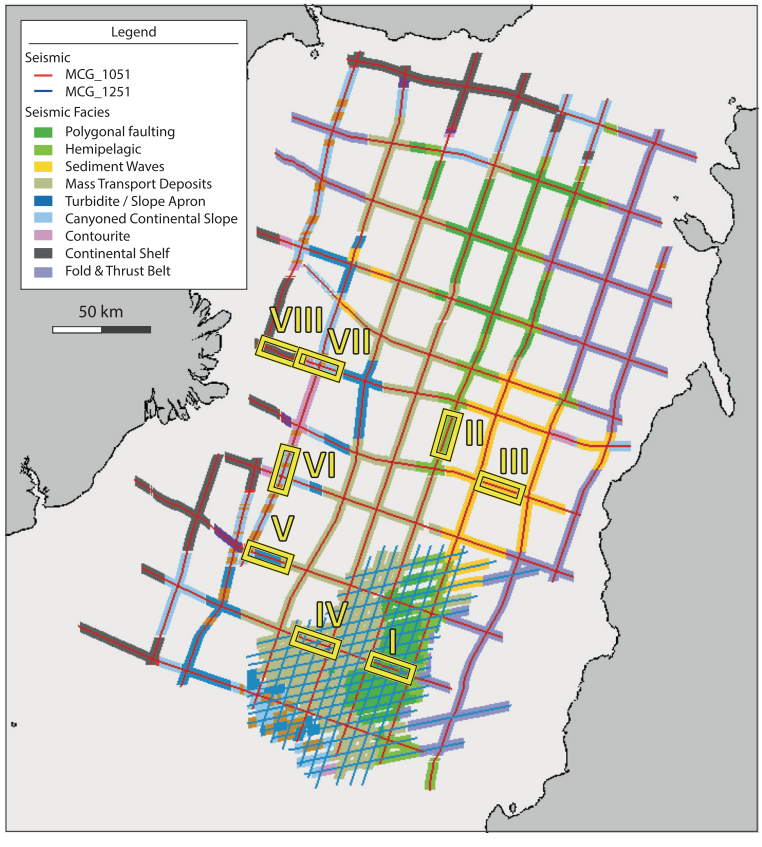

Fig. 8. Mapped seismic facies. Yellow boxes (I–VIII) indicate location of seismic sections shown in Figure 9.

SF V. Upslope of the MTDs and basin floor, SF V is characterized by subparallel and semi-continuous reflections (Fig. 9 V). Locally, this facies shows a mounded external morphology and thinning upslope. Reflections dip basinward but are at a lower angle than the seabed forming the upper continental slope. This facies is interpreted as a turbidite-dominated slope apron consisting of sediment fans and channel-levee systems.

SF VI. The upper slope shows varying seismic reflection amplitudes. Internally reflections are laterally semi-continuous, but commonly are truncated by downcutting, erosive canyons (Fig. 9 VI). Basinward-dipping reflections are seen in addition to mounded morphologies. Rare BSR reflections are also identified within SF VI.

SF VII. On the upper slope in the SW of the Makassar North Basin (Fig. 8), the SF is characterized by basinward-dipping, parallel, semi-continuous internal reflections (Fig. 9 VII), interpreted as contourites. The external morphology is distinctly convex up, with evidence of alongslope elongation (despite limited 2D data coverage). The upslope progradation of internal seismic reflections, combined with their external morphology, is typical of contourite-plastered drifts (Rebesco *et al.* 2014).

SF VIII. Characterized by horizontal to basinward-dipping, semi-parallel, discontinuous reflections, SF VIII is confined to the continental shelf (Fig. 9 VIII). Internal reflections are low amplitude, compared to the seabed reflection horizon (which locally is high amplitude), particularly in the north of the study area. Locally on the shelf or at the shelf break, isolated build-ups (Fig. 11a, b) are interpreted as biohermal carbonates (Roberts and Sydow 2003). These suggest that the locally high amplitude seabed seismic reflections are due to carbonate deposition.

Combining the observations and interpretations from the bathymetric and seismic mapping, an environment of deposition map for the Quaternary has been compiled (Fig. 12).

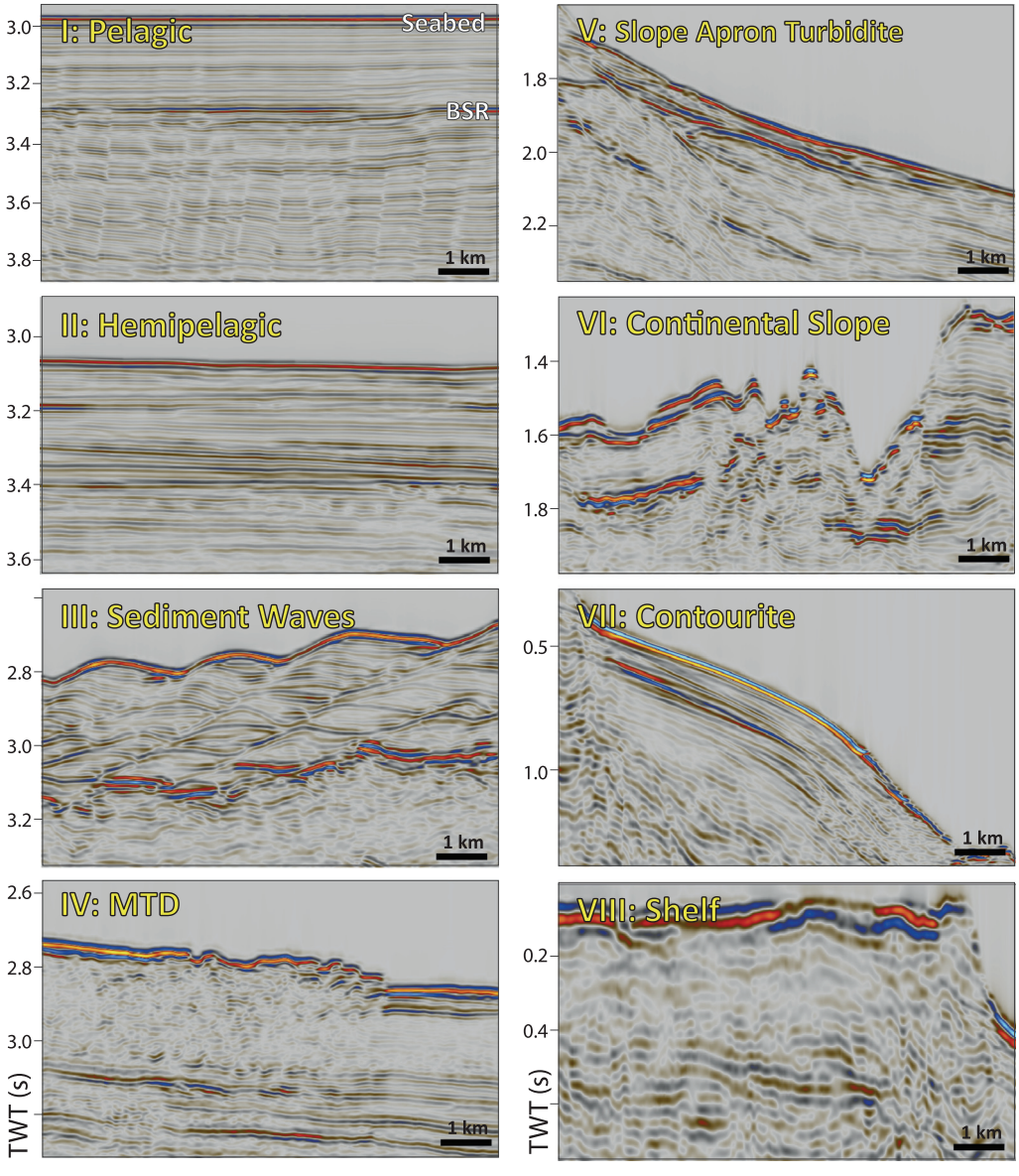

Fig. 9. Seismic facies of the Makassar Strait. Locations indicated on Figure 8.

MTDs. In total, 19 individual MTD deposits were mapped in detail (Table 2; Fig. 12), with volumes ranging from 5 km^3 to over 600 km^3 (Table 2). Five MTDs are over 100 km^3 in volume, with the three largest located at the base of the continental slope in the SW of the Makassar North Basin, south of the Mahakam Delta (Fig. 13). Mapping of internal and top-surface directional indicators (imbrications and lineations) reveals that the largest MTDs are sourced from the southwestern margin of the basin. Smaller (<50 km^3) events are sourced from the Mangkalihat High in the north and the Paternoster Platform in the south. No significant volume MTD events are identified in the fold-and-thrust belt – although numerous smaller events (<5 km^3) associated with thrust-cored anticlines are evident in the bathymetric data (e.g. Fig. 6b).

Based on their internal and external characteristics, the MTDs mapped in this study, are interpreted as deposited from translational submarine

Table 1. *Pliocene–Recent seismic facies (SF) across the Makassar Strait MCG surveys*

SF	Configuration and continuity	Amplitude and frequency	Bounding relationship	Depositional environment
I	Horizontal, parallel, discontinuous	High amplitude, high frequency	Fault-plane truncations. Laterally, merging with SF II	Pelagic with polygonal faulting
II	Horizontal, parallel, laterally continuous	High amplitude, high frequency	Laterally continuous, draping morphology	Hemipelagic
III	Hummocky, subparallel, semi-continuous	High amplitude, low frequency	Laterally continuous, onlapping upslope	Sediment waves
IV	Deformed – chaotic, discontinuous	Low amplitude, low frequency	Lenticular, basal erosional truncations and steps	MTDs
V	Dipping, subparallel, semi-continuous	Varied amplitude, mod. frequency	Localized mounded morphology. Thinning towards slope	Slope apron/ turbidite
VI	Dipping, subparallel, semi-continuous	Varied amplitude, low frequency	Canyon downcutting results in erosional truncation	Continental slope with canyons
VII	Dipping, parallel, semi-continuous	High amplitude, high frequency	Convex-upward lenticular. Elongate alongslope	Contourite
VIII	Horizontal, semi-parallel, discontinuous	Low amplitude, low frequency	High-amplitude top reflection with localized build-ups	Continental shelf

landslides. The isochron thickness map identifies a thin Pleistocene–Recent sequence in the upper slope which could be a possible failure zone (Fig. 7c). This suggests that the submarine landslides were initiated in the upper- to middle-continental slope between water depths of 500 and 1250 m.

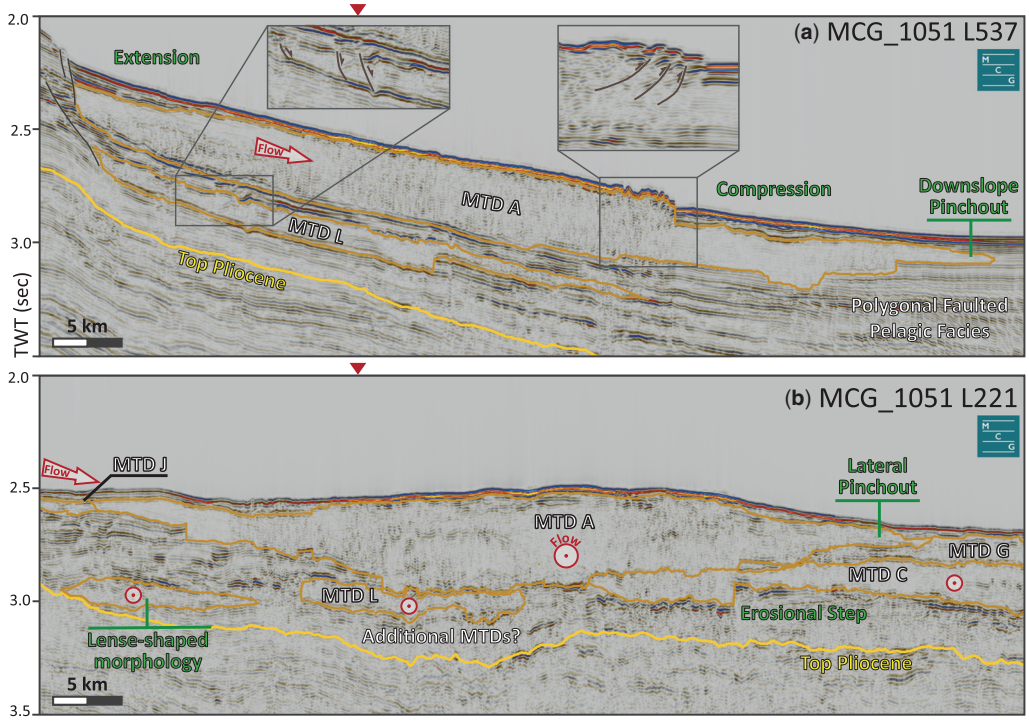

Fig. 10. Seismic character of MTDs in (**a**) dip and (**b**) strike. Location of section indicated in Figure 12. Red triangles indicate intersection. Flow direction in (b) towards the reader.

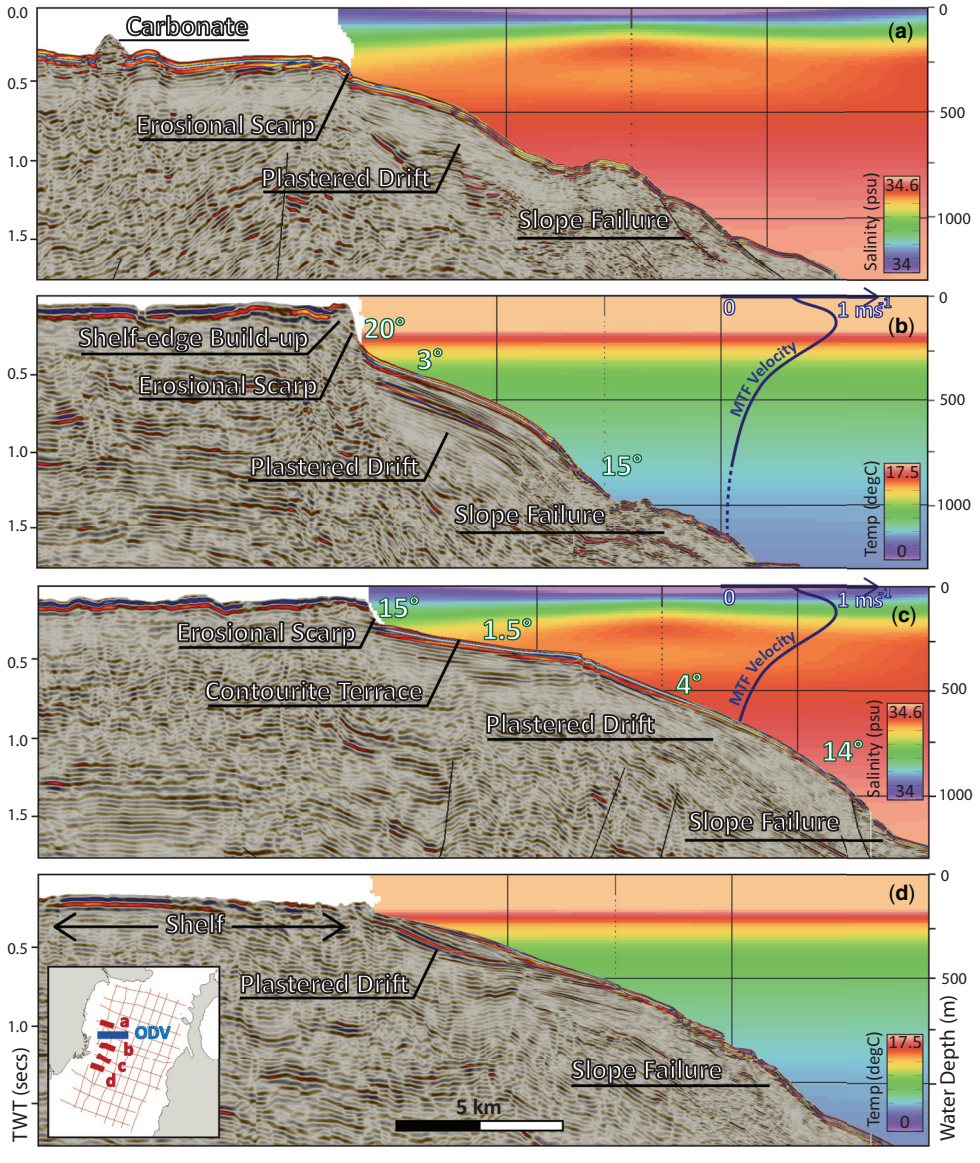

Fig. 11. Seismic character of the contourite depositional system across seismic line (**a**)–(**d**) indicated in inset map. Temperature and salinity data from Ocean Data View (ODV) section indicated (Schlitzer 2020). Slope gradients annotated in sections (b) and (c). Line locations indicated on Figure 12. Velocity–depth profile shows average velocity profile 2004–09 (Susanto *et al.* 2012).

Contourite features. On the upper slope, erosional and depositional contourite features are interpreted. Along the western edge of the Northern Basin, outboard of the shelf break there is a steep (15–20°) erosional escarpment that correlates well with the maximum velocity core of the MTF at 100–150 m water depth (Gordon *et al.* 2008). Locally, the base of this steep scarp is associated with a low gradient upper slope (1.5°) before a second shelf-slope break at 450 ms TWT (*c.* 300 m water depth). This is seen clearly on seismic line MCG_1051 L639 (Fig. 11b) where the 'step' in the upper slope corresponds to the average water depth of the base MTF at 300 m (Mayer and Damm 2012). It is therefore interpreted as a contourite terrace, formed by MTF erosion. The mechanisms for contourite terrace

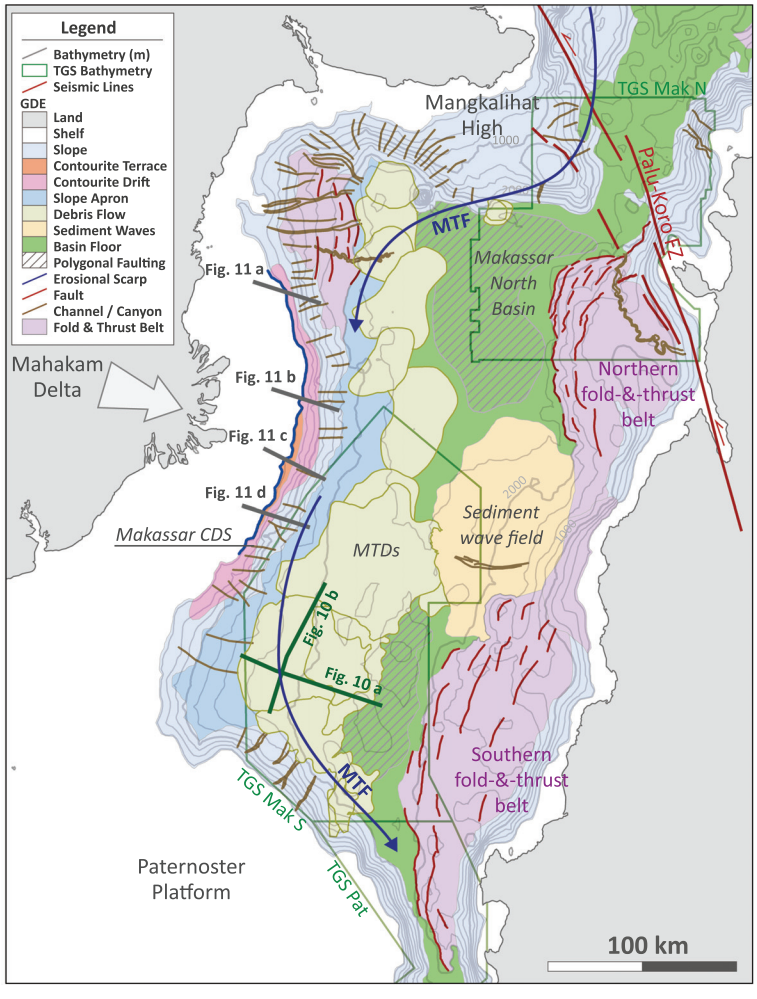

Fig. 12. Map of the environment of deposition of the Makassar North Basin. TGS bathymetry data extent indicates areas of high-resolution data. Additional information gathered from Fowler *et al.* (2004); Saller and Dharmasamadhi (2012); and Frederik *et al.* (2019). CDS, contourite depositional system.

formation are poorly understood (Hernández-Molina *et al.* 2008); however, the association between terrace depth and the base of the MTF suggests the possibility of enhanced current energy or internal wave-related erosion at the thermocline or pycnocline. The presence of an erosional scarp upslope of the terrace shows that this western boundary current is highly erosive in nature along much of the western margin of the Makassar North Basin. Downslope of the erosional features, SF VII shows a distinctly convex-upwards slope morphology, alongslope elongation and upslope progradation of internal reflections (Fig. 9) – all features diagnostic of contourites (Nielsen *et al.* 2008). We interpret these depositional features as plastered contourite drifts. In the Makassar South Basin, the Paternoster bathymetric data (Fig. 6) show a number of additional features that could represent contourites including: (1) an erosional scour orientated perpendicular to the Paternoster margin (Fig. 6a insert) – these scours are characterized by steep lee and shallow stoss sides, and are interpreted as formed by bottom current turbulence within the MTF on exiting the Labani Channel, similar to features described by Nicholson and Stow (2019); (2) a contourite terrace similar to that seen in the Makassar North Basin (Fig. 6b); and (3) a potential mounded drift within an embayment (Fig. 6a). However, additional seismic data are required to corroborate this interpretation.

Table 2. *Measurements from mapped MTDs and their calculated volumes*

MTD	Area (km^2)	Volume (TWT)	km^3 at 2000 m s^{-1}	Uncertainty (km^3) range ±
A	3410	616.47	616.47	123.29
B	938	53.88	53.88	10.78
C	3891	422.99	422.99	84.60
D	1482	110.60	110.60	22.12
E	1313	137.06	137.06	27.41
F	444	26.32	26.32	5.26
G	3959	212.19	212.19	42.44
H	230	41.87	41.87	8.37
I	193	5.85	5.85	1.17
J	882	50.57	50.57	10.11
K	249	12.71	12.71	2.54
L	660	58.64	58.64	11.73
M	523	36.81	36.81	7.36
N	865	57.56	57.56	11.51
O	963	75.64	75.64	15.13
P	659	42.48	42.48	8.50
Q	680	44.48	44.48	8.90
R	86	4.91	4.91	0.98
S	130	8.14	8.14	1.63

20% uncertainty range applied to allow for acoustic velocities between 1800 and 2200 m s^{-1}.

Discussion

Drivers for slope instability

There are a number of factors that contribute to instability of continental slopes: (1) seismic activity, including seismic loading and earthquake-related shaking; (2) slope oversteepening, due to erosion, carbonate build-up, faulting or diapirism; (3) loading, from water, sediments or ice – this can occur over various timescales, for example short-lived cyclic loading during storm events, or longer-term sea-level changes; (4) rapid accumulation and underconsolidation that can result in elevated pore pressures; and (5) gas hydrate disassociation (Locat and Lee 2002). All these processes act to either reduce the shear strength of continental slope sediments, or increase the stress acting upon them (Hampton *et al.* 1996). In addition, settings that result in steep seabed morphology such as fjords, volcanoes and carbonate build-ups are particularly susceptible to failure (Hampton *et al.* 1996). Here we discuss the possible drivers for slope failure in the Makassar Strait.

Carbonate build-up. Carbonate slopes are capable of reaching gradients that far exceed that of their siliciclastic counterparts (Schlager and Camber 1986). This ability to reach gradients of up to 29°, combined with their capacity to form a concave-upward slope morphology, makes them susceptible to mass failure (Hampton *et al.* 1996). Carbonates are present across the western margin of the Makassar Strait, both as isolated biohermal build-ups along the NW continental shelf, and more extensively across the Paternoster Platform in the SW. Based on kinematic indicators and gross morphology, a number of moderate size (<50 km^3) MTDs are sourced from the Paternoster Platform (Fig. 13). However, the largest MTDs are sourced from the western continental margin where clastic sedimentation from the Mahakam Delta dominates (Fig. 13), rather than the carbonate platform margin. It is therefore unlikely that oversteepening of carbonate slopes is a driver for large-scale submarine landslides in the Makassar North Basin.

Seismic activity. There is historical evidence for earthquake rupture of the seabed causing tsunamis (NGDC/WDS) and seismic activity is frequent across the Makassar Strait region (Fig. 1) (https://earthquake.usgs.gov/earthquakes), particularly in Sulawesi where earthquakes of up to M_w 8 are associated with the left lateral Palu-Koro fault zone (Fig. 1b). There are historical earthquakes along the eastern margin of the Makassar Strait; however, our mapping shows that the MTDs are sourced from the western margin. It is therefore unlikely that seismic activity and related seafloor fault rupture is the primary driver for these. Nevertheless, with the narrow Makassar Strait *c.* 300 km in width, it is possible that far-field seismic shaking is the *triggering* mechanism for submarine landslides of the Kalimantan continental margin. The distribution of the largest MTDs in the SW of the Makassar North Basin, away from historical earthquake epicentres, suggests that there is an additional *preconditioning* mechanism in this region for the generation of large-volume MTDs.

Deltaic deposition and sediment loading. A prominent sedimentary feature of the Kalimantan margin is the Mahakam Delta. With an estimated annual sediment discharge of 8×10^6 m^3 a^{-1} (Roberts and Sydow 2003), the Mahakam River provides significant volumes of sediment to this actively prograding delta. Delta fronts studied elsewhere (Hampton *et al.* 1996) are known to be vulnerable to collapse due to the interplay of various factors. For example, in the case of the Mississippi Delta, high sedimentation rates result in under-consolidated sediment accumulations and frequent failure (Coleman *et al.* 1993). Furthermore, these deltaic sediments are generally fine grained with high organic content and gas charge, which acts to reduce sediment shear strength. As a result, such sediments are preconditioned for failure.

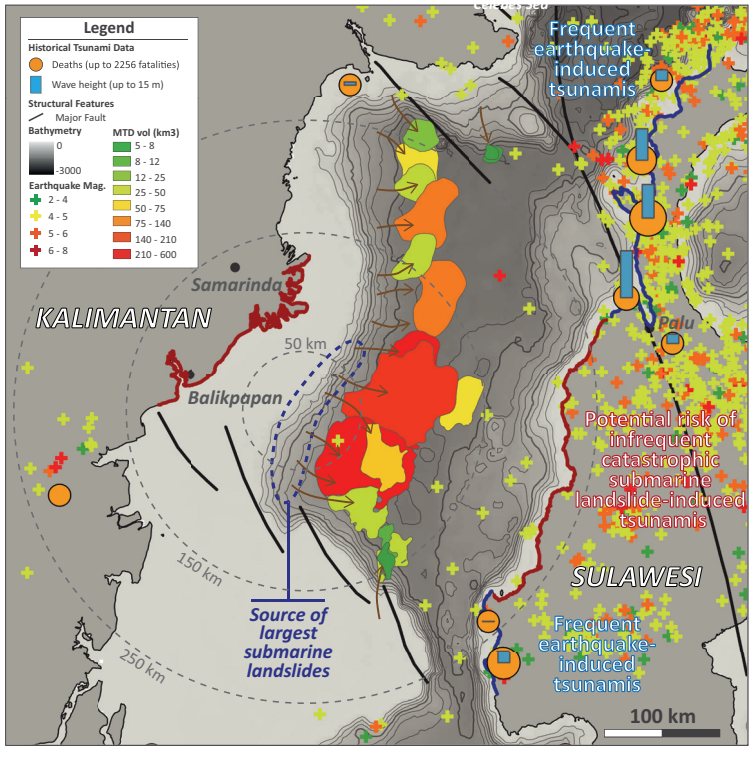

Fig. 13. Risk map showing the Makassar Throughflow. MTDs colour-coded with respect to their volume. Coastlines at risk of infrequent and catastrophic submarine landslide-induced tsunamis are indicated in red.

In the case of the Mahakam Delta, similar processes to those on the Mississippi Delta may promote mass failure of the continental slope. The Makassar Strait is a major oil and gas province, and sediments supplied to the delta are high in organic content (Saller *et al.* 2006) and therefore are likely to be low in shear strength. In addition, microbial consumption of organic matter and thermogenic maturation of kerogens is likely to result in methane production, which could reduce stability. Detailed interpretation of the seismic, bathymetry and gravity cores offshore the Mahakam Delta (Roberts and Sydow 2003) reveals that during Pleistocene lowstand conditions, delta growth occurred along the shelf-slope transition. This would have provided sediment directly to the upper slope, causing oversteepening and sediment loading, resulting in the slope being highly susceptible to failure. This situation explains why MTDs are distributed only along the western slope of the basin, unlike the eastern margin, where there is no comparable sediment influx. However, this observation does not explain the distribution of the largest mapped MTDs clustered to the SW of the Mahakam Delta (Fig. 13).

Slope failure preconditioning by the ITF. Mapping the present-day route of the MTF (Fig. 1c) shows that this western boundary current is interacting with the Kalimantan margin and the Mahakam Delta. Detailed mapping of the delta front shows the fine-grained prodelta (at *c.* 40 m water depth) is deflected to the south due to interaction with the MTF (Roberts and Sydow 2003). Regional gravity and depth to basement mapping (Cloke *et al.* 1999; Moss and Chambers 1999; Sandwell *et al.* 2014) demonstrate that the Mahakam depocentre has a marked asymmetry from north to south. Oceanographic measurements show the MTF current reaches 1 m s^{-1} within a subsurface 'jet' extending down to 300 m below the sea surface with a high velocity core at 100–150 m (Mayer and Damm 2012). Currents of this strength are sufficient to erode and transport sediments (Stow *et al.* 2008), as evidenced by the distribution of contourite erosional and depositional features across the upper slope of the Kalimantan margin, herein named the Makassar Contourite Depositional System (CDS) (Fig. 11).

Previous authors have highlighted that contourite deposition is often associated with slope instability

along continental margins (Laberg and Camerlenghi 2008; Stow *et al.* 2012; Miramontes *et al.* 2018; Nicholson *et al.* 2020). Along the NW European margin, the giant (*c.* 3500 km^3) Storegga Slide is, in part, a result of the reduced shear strength within the basal failure plane comprising clay-rich contourites (Bryn *et al.* 2005). In the South Falkland Basin, an over-steepened and basinward-dipping contourite drift on the Burdwood Bank has regularly failed due to upper-slope deposition and lower-slope erosion within a contourite moat (Nicholson *et al.* 2020). Along the East Canadian margin, MTDs are associated with shallow-water contourites (Rashid *et al.* 2017). A geotechnical review of these sediments concludes that their high fluid content, together with the highly cyclical nature of the sediments resulting in failure surfaces throughout the succession, may promote liquefaction from seismic shaking (Rashid *et al.* 2017). In these three regions, the cause of sediment failure is attributed to the nature and morphology of contourite sediments.

Thus, three key factors make contourites susceptible to mass transport failure. Firstly, the anomalously high sedimentation rates of contourite drifts reaching 60 cm ka^{-1} (Howe *et al.* 1994) can lead to high fluid content and elevated pore pressures upon burial. Secondly, the fine muddy nature of contourite sediments makes then likely to have low internal shear strength (Laberg and Camerlenghi 2008). Finally, their convex-upwards external morphology can locally result in high gradients on the continental slope making failure more likely (Stow *et al.* 2012; Miramontes *et al.* 2018). Laberg and Camerlenghi (2008) note that there is often an association between gas hydrate accumulation and contourite deposition due to the elevated pore space in these rapidly deposited sediments and may be an additional factor making contourites susceptible to failure.

In the case of the Makassar CDS, the high velocity MTF jet correlates well with the formation of a steep (20°) erosional scarp and relatively flat (1.5°) contourite terrace on the upper slope directly to the north and east of the Mahakam Delta (Fig. 11). This is evidence for the erosion and removal of sediments from this area, which are then transported and deposited downslope and downcurrent. This winnowing of sediments from the north results in enhanced sedimentation on the slope to the SE of the delta, directly above the region where the largest Quaternary MTDs have been mapped (Figs 12 & 13). Contourite-plastered drifts are identified along the margin, generally directly below the base of the MTF at 300 m water depth (Fig. 11). These regions of enhanced sedimentation are vulnerable to failure due to high fluid content, the high organic content of the Mahakam Delta sediments, and their convex-upwards morphology which results in an oversteepened, basinward-dipping slope, of around 15°. We propose these regions as the main source of mass transport sediments to the deep basin. It is noted that the plastered contourite drifts identified in this study are significantly smaller than examples seen along other passive continental margins (Hernández-Molina *et al.* 2008). We propose this to be a result of regular removal of material from the drifts during submarine landslide events.

The MTF is likely to have varied significantly in response to Quaternary climatic fluctuations, which may further play a role in controlling slope instability. The resolution of the data in our study, and the lack of well control, do not allow detailed evaluation of the timescales and the control of sea-level or climate on triggering these events, but it is expected that climate exerts a strong control on slope stability by controlling the depth, velocity and nature of the MTF. The evidence from previous studies, however, is conflicting. During glacial lowstands, much of the Paternoster Platform and the continental shelf was exposed (Hall 2009; Roberts and Sydow 2003), and the width and cross-sectional area of the Makassar Strait was considerably reduced. As a result, the MTF may have initially been accelerated due to flow constriction (Hall 2009). However, ocean-current velocity proxies suggest that the MTF was significantly reduced, or even switched off during glacial conditions (Gingele *et al.* 2002; Holbourn *et al.* 2011), due to the reduced exchange between the Pacific and South China seas (Godfrey 1996) and reduced Atlantic meridional overturning (Hendrizan *et al.* 2017). Modelling of the response of ocean currents to fluctuating sea-level in SE Asia is further complicated by the effect of monsoonal conditions on the region. Although the interplay between sea-level-induced restriction of the MTF and changes in velocity profile are not well understood, it is probable that sea-level fluctuations resulting from Pleistocene glacial–interglacial cyclicity affected slope instability. Further work is required to constrain variations in the timing and frequency of slope failure events to reveal the drivers.

Tsunamigenic risk

MTDs of the scale and volume mapped in this study in the Quaternary section of the Makassar North Basin, by analogy with other locations, would be expected to generate hazardous tsunamis (e.g. Harbitz *et al.* 2006; Tappin *et al.* 2008, 2014; Parsons *et al.* 2014) (Table 3). Many past large volume landslide tsunamis, such as Storegga, are prehistoric, and are recognized and mapped from their palaeo-record preserved in sediments (e.g. Dawson *et al.* 1988; Bondevik *et al.* 1997). There is no historical evidence for tsunamis originating in the

Table 3. *Key characteristics of previous tsunamigenic submarine landslides*

Tsunami	MTD volume (km^3)	Water depth (m)	Initial acceleration ($m\ s^{-1}$)	Distance to shore (km)	Run up (m)	Reference
PNG	4	1200	0.47	25	10–15	Tappin *et al.* (2008)
Japan	500	4000–5500	0.37	150	40	Tappin *et al.* (2014)
Falklands	100	860	0.37	180	40	Nicholson *et al.* (2020)
Grand Banks*	200	500	unknown	340	13	Fine *et al.* (2005)
Makassar Strait	100–600 km^3	500–1000	unknown	E = 180; W = 100	unknown	

*Grand Banks reverse wave documented.

Makassar Strait, and no one has yet looked for evidence of prehistoric (Pleistocene–Recent) events. This leads us to conclude that either: (1) the submarine landslides that generated these MTDs were not tsunamigenic; or (2) tsunamis generated by submarine landslides are of much lower frequency than those generated by fault movements and have not occurred since historical records began. This needs to be tested by investigating evidence for palaeo-tsunamis in the surrounding coastal regions, although evidence is only likely to be preserved for Holocene–Recent events.

From our tentative chronology of the MTDs sourced from the Mahakam Delta, they have occurred frequently throughout the Quaternary. A conservative estimate of the frequency of submarine landslides $>100\ km^3$ is approximately every 0.5 Ma. Events larger than $10\ km^3$ are conservatively estimated to have occurred every 160 ka; detailed mapping of high-resolution 3D seismic surveys would likely reveal multiple smaller events and a significantly higher frequency. It is, however, likely that the last large-scale failure event occurred prior to historical records. If the landslides were tsunamigenic, they would impact the local Sulawesi and Kalimantan coastlines which previously were not considered at risk of tsunamis. There are a number of towns along the Sulawesi coast, *c.* 180 km east and directly in front of the largest MTD deposits that could be affected by any forward-propagating wave. The distance is comparable to that travelled by previous tsunamis in Papua New Guinea (Tappin *et al.* 2008) and Japan (Tappin *et al.* 2014) (Table 3). The high-energy point source release of tsunamis from submarine landslides also generates a significant reverse wave, travelling in the opposite direction to slope failure. This reverse wave would travel only 100 km before reaching the low-lying cities of Balikpapan (population >850 000) and Samarinda (population >840 000). The destructive nature of such a reverse wave was demonstrated in the 1929 Grand Banks event, when a 13 m wave struck the Newfoundland Coast following a slope failure some 340 km offshore (Fine *et al.* 2005). With the exception of distance to shoreline, the characteristics of the Grand Banks slope failure (MTD volume and water depth) are similar to the MTDs mapped in the Makassar Strait. Therefore, if the Makassar Strait submarine landslides were capable of generating tsunami waves, it is expected that the back-wave could also form a tsunami risk, with local morphological features such as channels and estuaries, including Balikpapan Bay further amplifying the wave height.

Tsunamis generated by submarine landslides differ in character from those sourced from fault rupture of the seabed (Okal and Synolakis 2003). Unlike the linear wave formed by fault rupture (Aida 1978; Tanioka and Satake 1996), landslides generate a tsunami wave from a point source that radially spreads out in the direction of the submarine failure, with a negative reverse wave spreading in the opposite direction (Harbitz *et al.* 2006). The magnitude of the wave is much larger than those formed by fault rupture; however, rapid radial dampening limits the destructive distance of the tsunami (Okal and Synolakis 2003). The magnitude of a tsunami generated by a submarine landslide is strongly controlled by landslide volume, initial acceleration and the water depth of initial failure (Harbitz *et al.* 2006). Tsunami wave modelling is urgently required to test slope failure scenarios and identify any coastal regions at risk. This will allow for the potential risk to be quantified, and inform recommendations for mitigation measures to be put into effect and evacuation plans be implemented in high-risk regions.

Conclusions

This study identifies, for the first time, multiple large-volume MTDs generated by submarine landslides within the Quaternary section of the Makassar North Basin. The largest MTDs are clustered in the SW of the basin and are over $600\ km^3$ in volume.

Kinematic indicators demonstrate that the MTDs are sourced from the western margin of the Makassar Strait, south of the Mahakam Delta. Mapping along this western margin also reveals a contourite depositional system along the upper slope: the Makassar CDS.

We propose that the largest and most frequent submarine landslides in the Makassar North Basin are genetically related to these contourites. Sediments transported into the basin from the Mahakam Delta are redistributed by the MTF and deposited on the upper slope to the south of the delta, resulting in elevated sedimentation rates in this region. In combination with fine grain size, rapid burial promotes fluid retention and overpressure generation, increasing the probability of slope failure. The fine, muddy nature of the drifts makes them likely to have low shear strength, and their convex-upwards morphology results in locally high gradients on the upper continental slope. All of these factors make these deposits inherently unstable and prone to failure.

Based on analogue studies of MTDs elsewhere, it is probable that the submarine landslides that generated the mapped deposits were tsunamigenic. The wave generated from the submarine landslides mapped in this study could impact the Sulawesi and Kalimantan coastlines in regions not previously affected by historical events. It is therefore critical to understand the triggering mechanisms of these events and their hazard. Future work will aim to constrain the frequency, and the role of climate and sea-level on submarine landslide triggering. Tsunami wave modelling is required to test slope failure scenarios and identify coastal regions at highest risk.

Acknowledgements We would like to thank our partners at Bandung Institute of Technology, and the members of the Indonesian Marine Geological Institute and Geological Survey of Indonesia for their discussion and contribution to this research. We thank TGS and Multiclient Geophysical for permission to publish seismic and multibeam data respectively. D.R. Tappin publishes with the permission of the Executive Director of the BGS (United Kingdom Research and Innovation).

Funding This work was completed as part of a Scottish Funding Council (SFC) Global Challenges Research Fund (GCRF) pump-priming project at Heriot Watt University (PI Nicholson).

Author contributions **REB**: formal analysis (lead), investigation (lead), writing – original draft (lead); **UN**: conceptualization (lead), funding acquisition (lead), supervision (lead), writing – review & editing (lead); **BS**: funding acquisition (equal), validation (supporting); **DS**: conceptualization (supporting), funding acquisition (supporting), supervision (supporting), writing – review & editing (supporting); **DRT**: funding acquisition (equal), validation (supporting), writing – review & editing (supporting).

References

Aida, I. 1978. Reliability of a tsunami source model derived from fault parameters. *Journal of Physics of the Earth*, **26**, 57–73, https://doi.org/10.4294/jpe1952.26.57

Becker, J.J.D.T., Sandwell, W.H.F. *et al*. 2009. Global Bathymetry and Elevation Data at 30 Arc Seconds Resolution: SRTM30_PLUS. *Marine Geodesy*, **32**, 355–371, https://doi.org/10.1080/01490410903297766

Bergman, S.C., Coffield, D.Q., Talbot, J.P. and Garrard, R.A. 1996. Tertiary tectonic and magmatic evolution of western Sulawesi and the Makassar Strait, Indonesia: evidence for a Miocene continent-continent collision. *Geological Society, London, Special Publications*, **106**, 391–429, https://doi.org/10.1144/GSL.SP.1996.106.01.25

Bird, M.I., Taylor, D. and Hunt, C. 2005. Palaeoenvironments of insular Southeast Asia during the Last Glacial Period: a savanna corridor in Sundaland? *Quaternary Science Reviews*, **24**, 2228–2242, https://doi.org/10.1016/j.quascirev.2005.04.004

Bondevik, S., Svendsen, J.I., Johnsoen, G., Mangerud, J.A.N. and Kaland, P.E. 1997. The Storegga tsunami along the Norwegian coast, its age and run up. *Boreas*, **26**, 29–53, https://doi.org/10.1111/j.1502-3885.1997.tb00649.x

Bryn, P., Berg, K., Forsberg, C.F., Solheim, A. and Kvalstad, T.J. 2005. Explaining the Storegga slide. *Marine and Petroleum Geology*, **22**, 11–19, https://doi.org/10.1016/j.marpetgeo.2004.12.003

Burollet, P.F., Boichard, R., Lambert, B. and Villain, J.M. 1986. The Pater Noster Carbonate Platform. *Indonesian Petroleum Association 15th Annual Convention Proceedings*, **1**, 155–169.

Carvajal, M., Araya-Cornejo, C., Sepúlveda, I., Melnick, D. and Haase, J.S. 2019. Nearly instantaneous tsunamis following the Mw 7.5 2018 Palu earthquake. *Geophysical Research Letters*, **46**, 5117–5126, https://doi.org/10.1029/2019GL082578

Cloke, I.R., Milsom, J. and Blundell, D.J.B. 1999. Implications of gravity data from East Kalimantan and the Makassar Straits: a solution to the origin of the Makassar Straits? *Journal of Asian Earth Sciences*, **17**, 61–78, https://doi.org/10.1016/S0743-9547(98)00056-7

Coleman, J.M., Prior, D.B., Garrison, L.E. and Lee, H. 1993. Slope failures in an area of high sedimentation rate: Offshore Mississippi River delta. *In*: Schwab, W.C., Lee, H.J. and Twichell, D.C. (eds) *Submarine Landslides: Selected Studies in the US Exclusive Economic Zone*. US Geological Survey Bulletin, **2002**, 79–91.

Daly, M.C., Cooper, M.A., Wilson, I., Smith, D.G. and Hooper, B.G.D. 1991. Cenozoic plate tectonics and basin evolution in Indonesia. *Marine and Petroleum Geology*, **8**, 2–21, https://doi.org/10.1016/0264-8172(91)90041-X

Davies, R.J. and Ireland, M.T. 2011. Initiation and propagation of polygonal fault arrays by thermally triggered volume reduction reactions in siliceous sediment.

Marine Geology, **289**, 150–158, https://doi.org/10.1016/j.margeo.2011.05.005

Dawson, A.G., Long, D. and Smith, D.E. 1988. The Storegga slides: evidence from eastern Scotland for a possible tsunami. *Marine Geology*, **82**, 271–276, https://doi.org/10.1016/0025-3227(88)90146-6

Decker, J., Teas, P.A., Schneider, R.D., Saller, A.H. and Orange, D.L. 2004. Modern deep-sea sedimentation in the Makassar Strait: insights from high-resolution multibeam bathymetry and backscatter, sub-bottom profiles, and USBL-navigated cores. *In*: Noble, R.A., Argenton, A. and Caughey, C.A. (eds) *Deepwater and Frontier Exploration in Asia & Australasia*. Proceedings of the International Geoscience Conference, Indonesian Petroleum Association, Jakarta, DFE-04-PO-042, 377–387.

Del Negro, R., Castellano, P., Kuhfuss, A., Mattioni, L., Moss, J. and Vialla, M. 2013. Structural Styles and Petroleum System Modelling of the North Makassar Straits, Indonesia. *Proceedings of the Indonesian Petroleum Association Thirty-Seventh Annual Convention & Exhibition*, May 2013, Jakarta, IPA13-G-077.

Fine, I.V., Rabinovich, A.B., Bornhold, B.D., Thomson, R.E. and Kulikov, E.A. 2005. The Grand Banks landslide-generated tsunami of November 18, 1929: preliminary analysis and numerical modeling. *Marine Geology*, **215**, 45–57, https://doi.org/10.1016/j.margeo.2004.11.007

Fowler, J.N., Guritno, E. *et al*. 2004. Depositional architectures of recent deepwater deposits in the Kutei Basin, East Kalimantan. *Geological Society, London, Memoirs*, **29**, 25–34, https://doi.org/10.1144/GSL.MEM.2004.029.01.03

Frederik, M.C., Adhitama, R. *et al*. 2019. First results of a bathymetric survey of Palu Bay, Central Sulawesi, Indonesia following the Tsunamigenic Earthquake of 28 September 2018. *Pure and Applied Geophysics*, **176**, 3277–3290, https://doi.org/10.1007/s00024-019-02280-7

Gingele, F.X., De Deckker, P., Girault, A. and Guichard, F. 2002. History of the South Java Current over the past 80 ka. *Palaeogeography, Palaeoclimatology, Palaeoecology*, **183**, 247–260, https://doi.org/10.1016/S0031-0182(01)00489-8

Godfrey, J.S. 1996. The effect of the Indonesian throughflow on ocean circulation and heat exchange with the atmosphere: a review. *Journal of Geophysical Research: Oceans*, **101**, 12217–12237, https://doi.org/10.1029/95JC03860

Gordon, A.L. and Fine, R.A. 1996. Pathways of water between the Pacific and Indian oceans in the Indonesian seas. *Nature*, **379**, 146, https://doi.org/10.1038/379146a0

Gordon, A.L., Susanto, R.D., Field, A., Huber, B.A., Pranowo, W. and Wirasantosa, S. 2008. Makassar Strait throughflow, 2004 to 2006. *Geophysical Research Letters*, **35**, https://doi.org/10.1029/2008GL036372

Grilli, S.T., Tappin, D.R. *et al*. 2019. Modelling of the tsunami from the December 22, 2018 lateral collapse of Anak Krakatau volcano in the Sunda Straits, Indonesia. *Scientific Reports*, **9**, 1–13, https://doi.org/10.1038/s41598-019-48327-6

Guntoro, A. 1999. The formation of the Makassar Strait and the separation between SE Kalimantan and SW Sulawesi. *Journal of Asian Earth Sciences*, **17**, 79–98, https://doi.org/10.1016/S0743-9547(98)00037-3

Hall, R. 1997. Cenozoic plate tectonic reconstructions of SE Asia. *Geological Society, London, Special Publications*, **126**, 11–23, https://doi.org/10.1144/GSL.SP.1997.126.01.03

Hall, R. 2009. Southeast Asia's changing palaeogeography. *Blumea-Biodiversity, Evolution and Biogeography of Plants*, **54**, 148–161, https://doi.org/10.3767/000651909X475941

Hall, R., Ali, J.R., Anderson, C.D. and Baker, S.J. 1995. Origin and motion history of the Philippine Sea Plate. *Tectonophysics*, **251**, 229–250, https://doi.org/10.1016/0040-1951(95)00038-0

Hall, R., Cloke, I.R., Nur'aini, S., Puspita, S.D., Calvert, S.J. and Elders, C.F. 2009. The North Makassar Straits: what lies beneath? *Petroleum Geoscience*, **15**, 147–158, https://doi.org/10.1144/1354-079309-829

Hampton, M.A., Lee, H.J. and Locat, J. 1996. Submarine landslides. *Reviews of Geophysics*, **34**, 33–59, https://doi.org/10.1029/95RG03287

Harbitz, C.B., Løvholt, F., Pedersen, G. and Masson, D.G. 2006. Mechanisms of tsunami generation by submarine landslides: a short review. *Norwegian Journal of Geology/Norsk Geologisk Forening*, **86**, 255–265.

Hendrizan, M., Kuhnt, W. and Holbourn, A. 2017. Variability of Indonesian Throughflow and Borneo runoff during the last 14 kyr. *Paleoceanography*, **32**, 1054–1069, https://doi.org/10.1002/2016PA003030

Hernández-Molina, F.J., Llave, E. and Stow, D.A.V. 2008. Continental slope contourites. *Developments in Sedimentology*, **60**, 379–408, https://doi.org/10.1016/S0070-4571(08)10019-X

Holbourn, A., Kuhnt, W. and Xu, J. 2011. Indonesian Throughflow variability during the last 140 ka: the Timor outflow. *Geological Society, London, Special Publications*, **355**, 283–303, https://doi.org/10.1144/SP355.14

Howe, J.A., Stoker, M.S. and Stow, D.A.V. 1994. Late Cenozoic sediment drift complex, northeast Rockall Trough, North Atlantic. *Paleoceanography*, **9**, 989–999, https://doi.org/10.1029/94PA01440

Jamelot, A., Gailler, A., Heinrich, P., Vallage, A. and Champenois, J. 2019. Tsunami simulations of the Sulawesi M w 7.5 event: Comparison of seismic sources issued from a tsunami warning context v. post-event finite source. *Pure and Applied Geophysics*, **176**, 3351–3376, https://doi.org/10.1007/s00024-019-02274-5

Katili, J.A. 1975. Volcanism and plate tectonics in the Indonesian island arcs. *Tectonophysics*, **26**, 165–188, https://doi.org/10.1016/0040-1951(75)90088-8

Koop, H., Flueh, E.R., Petersen, C.J., Weinrebe, W. and Wittwer, A., Meramex Scientists 2006. The Java margin revisited: Evidence for the subduction erosion off Java. *Earth and Planetary Science Letters*, **242**, 130–142, https://doi.org/10.1016/j.epsl.2005.11.036

Kuhnt, W., Holbourn, A., Hall, R., Zuvela, M. and Käse, R. 2004. Neogene history of the Indonesian throughflow. Continent-Ocean Interactions within East Asian Marginal Seas. *Geophysical Monograph*, **149**, 299–320, https://doi.org/10.1029/149GM16

Laberg, J.S. and Camerlenghi, A. 2008. The significance of contourites for submarine slope stability. *Developments*

in Sedimentology, **60**, 537–556, https://doi.org/10.1016/S0070-4571(08)10025-5

Lee, G.H., Kim, H.J., Jou, H.T. and Cho, H.M. 2003. Opal-A/opal-CT phase boundary inferred from bottom-simulating reflectors in the southern South Korea Plateau, East Sea (Sea of Japan). *Geophysical Research Letters*, **30**, https://doi.org/10.1029/2003GL018670

Locat, J. and Lee, H.J. 2002. Submarine landslides: advances and challenges. *Canadian Geotechnical Journal*, **39**, 193–212, https://doi.org/10.1139/t01-089

Mayer, B. and Damm, P.E. 2012. The Makassar Strait throughflow and its jet. *Journal of Geophysical Research: Oceans*, **117**, https://doi.org/10.1029/2011JC007809

McCloskey, J., Antonioli, A. *et al*. 2008. Tsunami threat in the Indian Ocean from a future megathrust earthquake west of Sumatra. *Earth and Planetary Science Letters*, **265**, 61–81, https://doi.org/10.1016/j.epsl.2007.09.034

Miramontes, E., Garziglia, S., Sultan, N., Jouet, G. and Cattaneo, A. 2018. Morphological control of slope instability in contourites: a geotechnical approach. *Landslides*, **15**, 1085–1095, https://doi.org/10.1007/s10346-018-0956-6

Moss, S.J. and Chambers, J.L. 1999. Tertiary facies architecture in the Kutai basin, Kalimantan, Indonesia. *Journal of Asian Earth Sciences*, **17**, 157–181, https://doi.org/10.1016/S0743-9547(98)00035-X

NGDC/WDS National Geophysical Data Center/World Data Service: NCEI/WDS Global Historical Tsunami Database. NOAA National Centers for Environmental Information, https://doi.org/10.7289/V5PN93H7 [last accessed May 2019].

Nicholson, U. and Stow, D. 2019. Erosion and deposition beneath the Subantarctic Front since the Early Oligocene. *Scientific Reports*, **9**, https://doi.org/10.1038/s41598-019-45815-7

Nicholson, U., Libby, S., Tappin, D.R. and McCarthy, D. 2020. The Subantarctic Front as a sedimentary conveyor belt for tsunamigenic submarine landslides. *Marine Geology*, **424**, 106161, https://doi.org/10.1016/j.margeo.2020.106161

Nielsen, T., Knutz, P.C. and Kuijpers, A. 2008. Seismic expression of contourites depositional systems. *Developments in Sedimentology*, **60**, 379–408, https://doi.org/10.1016/S0070-4571(08)10019-X

Okal, E.A. and Synolakis, C.E. 2003. A theoretical comparison of tsunamis from dislocations and landslides. *Pure and Applied Geophysics*, **160**, 2177–2188, https://doi.org/10.1007/s00024-003-2425-x

Okal, E.A. and Synolakis, C.E. 2008. Far-field tsunami hazard from mega-thrust earthquakes in the Indian Ocean. *Geophysical Journal International*, **172**, 995–1015, https://doi.org/10.1111/j.1365-246X.2007.03674.x

Parsons, T., Geist, E.L. *et al*. 2014. Source and progression of a submarine landslide and tsunami: The 1964 Great Alaska earthquake at Valdez. *Journal of Geophysical Research: Solid Earth*, **119**, 8502–8516, https://doi.org/10.1002/2014JB011514

Posamentier, H.W. and Meizarwin, W.T. 2000. Deep water depositional systems–ultra-deep Makassar Strait, Indonesia. *GCSSEPM Foundation 20th Annual Research Conference Deep-Water Reservoirs of the World*, **3** (6), 806–816.

Prasetya, G.S., De Lange, W.P. and Healy, T.R. 2001. The Makassar Strait tsunamigenic region, Indonesia. *Natural Hazards*, **24**, 295–307, https://doi.org/10.1023/A:1012297413280

Puspita, S.D., Hall, R. and Elders, C.F. 2005. Structural styles of the offshore West Sulawesi fold belt, North Makassar Straits, Indonesia. *Proceedings of the Indonesian Petroleum Association Thirtieth Annual Convention & Exhibition*, August 2005, Jakarta, 519–542, IPA05-G-110.

Rahmstorf, S. 2007. Thermohaline circulation. *In*: Elias, S.A. (ed.) *Encyclopedia of Quaternary Sciences*, 739–750, Elsevier, https://doi.org/10.1016/B0-44-452747-8/00014-4

Rashid, H., MacKillop, K., Sherwin, J., Piper, D.J.W., Marche, B. and Vermooten, M. 2017. Slope instability on a shallow contourite-dominated continental margin, southeastern Grand Banks, eastern Canada. *Marine Geology*, **393**, 203–215, https://doi.org/10.1016/j.margeo.2017.01.001

Rebesco, M., Hernández-Molina, F.J., Van Rooij, D. and Wåhlin, A. 2014. Contourites and associated sediments controlled by deep-water circulation processes: state-of-the-art and future considerations. *Marine Geology*, **352**, 111–154, https://doi.org/10.1016/j.margeo.2014.03.011

Roberts, H.H. and Sydow, J. 2003. Late Quaternary stratigraphy and sedimentology of the offshore Mahakam delta, east Kalimantan (Indonesia). *SEPM Special Publication*, **76**, 125–145, https://doi.org/10.2110/pec.03.76.0125

Ryan, W.B.F., Scarbotte, S.M. *et al*. 2009. Global Multi-Resolution Topography synthesis. *Geochemistry Geophysics, Geosystems*, **10**, Q03014, https://doi.org/10.1029/2008GC002332

Saller, A. and Dharmasamadhi, I.N.W. 2012. Controls on the development of valleys, canyons, and unconfined channel–levee complexes on the Pleistocene Slope of East Kalimantan, Indonesia. *Marine and Petroleum Geology*, **29**, 15–34, https://doi.org/10.1016/j.marpetgeo.2011.09.002

Saller, A., Lin, R. and Dunham, J. 2006. Leaves in turbidite sands: The main source of oil and gas in the deep-water Kutei Basin, Indonesia. *AAPG Bulletin*, **90**, 1585–1608, https://doi.org/10.1306/04110605127

Saller, A., Werner, K., Sugiaman, F., Cebastiant, A., May, R., Glenn, D. and Barker, C. 2008. Characteristics of Pleistocene deep-water fan lobes and their application to an upper Miocene reservoir model, offshore East Kalimantan, Indonesia. *AAPG Bulletin*, **92**, 919–949, https://doi.org/10.1306/03310807110

Schlager, W. and Camber, O. 1986. Submarine slope angles, drowning unconformities, and self-erosion of limestone escarpments. *Geology*, **14**, 762–765, https://doi.org/10.1130/0091-7613(1986)14<762:SSADUA>2.0.CO;2

Sandwell, D.T., Müller, R.D., Smith, W.H.F., Garcia, E. and Francis, R. 2014. New global marine gravity model from CryoSat-2 and Jason-1 reveals buried tectonic structure. *Science*, **346**, 65–67, https://doi.org/10.1126/science.1258213

Sangadji, R. 2019. Central Sulawesi disasters killed 4340 people, final count reveals. *Jakarta Post*, retrieved 16 September 2019.

Schlitzer, R. 2020. Ocean Data View, ODV 5.2.1, http://odv.awi.de

Stow, D.A.V., Hunter, S., Wilkinson, D. and Hernández-Molina, F.J. 2008. The nature of contourite deposition. *Developments in Sedimentology*, **60**, 143–156, https://doi.org/10.1016/S0070-4571(08)10009-7

Stow, D.A.V., Brackenridge, R., Patel, U. and Toulmin, S. 2012. Geohazards and ocean hazards in deepwater: overview and methods of assessment. Paper OTC 23697, presented at the Offshore Technology Conference, Houston.

Susanto, R.D. and Gordon, A.L. 2005. Velocity and transport of the Makassar Strait throughflow. *Journal of Geophysical Research: Oceans*, **110**, https://doi.org/10.1029/2004JC002425

Susanto, R.D., Field, A., Gordon, A.L. and Adi, T.R. 2012. Variability of Indonesian throughflow within Makassar Strait, 2004–2009. *Journal of Geophysical Research: Oceans*, **117**, https://doi.org/10.1029/2012JC008096

Takagi, H., Pratama, M.B., Kurobe, S., Esteban, M., Aránguiz, R. and Ke, B. 2019. Analysis of generation and arrival time of landslide tsunami to Palu City due to the 2018 Sulawesi Earthquake. *Landslides*, **16**, 983–991, https://doi.org/10.1007/s10346-019-01166-y

Tanioka, Y. and Satake, K. 1996. Tsunami generation by horizontal displacement of ocean bottom. *Geophysical Research Letters*, **23**, 861–864, https://doi.org/10.1029/96GL00736

Tappin, D.R., Watts, P. and Grilli, S.T. 2008. The Papua New Guinea tsunami of 17 July 1998: anatomy of a catastrophic event. *Natural Hazards and Earth System Science*, **8**, 243–266, https://doi.org/10.5194/nhess-8-243-2008

Tappin, D.R., Grilli, S.T. *et al*. 2014. Did a submarine landslide contribute to the 2011 Tohoku tsunami? *Marine Geology*, **357**, 344–361, https://doi.org/10.1016/j.margeo.2014.09.043

Tillinger, D. 2011. Physical oceanography of the present day Indonesian Throughflow. *Geological Society, London, Special Publications*, **355**, 267–281, https://doi.org/10.1144/SP355.13

Williams, R., Rowley, P. and Garthwaite, M.C. 2019. Reconstructing the Anak Krakatau flank collapse that caused the December 2018 Indonesian tsunami. *Geology*. **47**, 973–976, https://doi.org/10.1130/G46517.1

Yalciner, A.C., Hidayat, R. *et al*. 2018. Field Survey on the Coastal Impacts of the September 28, 2018 Palu, Indonesia Tsunami. *AGU Fall Meeting Abstracts*, 10–14 December 2018, Washington D.C. Walter E Washington Convention Center.